

The Superbubble Size Distribution in the Interstellar Medium of Galaxies

M. S. Oey^{*} and C. J. Clarke^{*}

Institute of Astronomy, University of Cambridge, Madingley Road, Cambridge CB3 0HA

Accepted 1997 March 03. Received 1996 December 10; in original form 1996 December 10

ABSTRACT

We use the standard, adiabatic shell evolution to predict the differential size distribution $N(R)$ for populations of OB superbubbles in a uniform ISM. Assuming that shell growth stalls upon pressure equilibrium with the ambient ISM, we derive $N(R)$ for simple cases of superbubble creation rate and mechanical luminosity function (MLF). For constant creation and an MLF $\phi(L) \propto L^{-\beta}$, we find that $N(R) \propto R^{1-2\beta}$ for $R < R_e$, and $N(R) \propto R^{4-5\beta}$ for $R > R_e$, where the characteristic radius $R_e \sim 1300$ pc for typical ISM parameters. For $R < R_e$, $N(R)$ is dominated by stalled objects, while for $R > R_e$ it is dominated by growing objects. The relation $N(R) \propto R^{1-2\beta}$ appears to be quite robust, and also results from momentum-conserving shell evolution. We predict a peak in $N(R)$ corresponding to individual SNRs, and suggest that the contribution of Type Ia SNRs should be apparent in the observed form of $N(R)$. We present expressions for the porosity parameters, Q_{2D} and Q_{3D} , derived from our analysis. Q_{2D} is dominated by the largest superbubbles for $\beta < 2$ and individual SNRs for $\beta > 2$, whereas Q_{3D} is normally dominated by the few largest shells.

We examine evolutionary effects on the H II region luminosity function (H II LF), in order to estimate β . We find that for a nebular luminosity fading with time t , $\mathcal{L} \propto t^{-\eta}$, there is a minimum observed slope a_{\min} for the H II LFs. Empirical measurements all show $a > a_{\min}$, therefore implying that usually we may take $\beta = a$. We also find that if nebular luminosity is instantaneously extinguished at some given age, rather than continuously fading, no a_{\min} will be observed.

Comparison with the largely complete HI hole catalog for the SMC shows surprising agreement in the predicted and observed slope of $N(R)$. This suggests that no other fundamental process is needed to explain the size distribution of shells in the SMC. Further comparison with largely incomplete HI data for M31, M33, and Holmberg II also shows agreement in the slopes, but perhaps hinting at systematic differences between spiral and Im galaxies. We estimate porosities that are substantially < 1 for all of the galaxies except Holmberg II, for which we obtain values $\gtrsim 1$. Most of these galaxies therefore may not be strongly dominated by a hot interstellar component. However, porosity results for the Galaxy remain inconclusive with the available data.

Key words: ISM: bubbles — ISM: general — H II regions — ISM: structure — supernova remnants — galaxies: ISM — galaxies: individual: SMC

1 INTRODUCTION

The evolution of superbubbles created by the stellar winds and supernovae of OB associations is one of the primary processes that determines the structure and energetics of the interstellar medium (ISM). All components of the diffuse interstellar

^{*} Email: oey@ast.cam.ac.uk (MSO); cclarke@ast.cam.ac.uk (CJC).

medium, including warm and cold HI as well as the warm ionized medium (WIM), are thought to have large fractions of their volume consisting largely of superbubble walls (*e.g.*, Heiles 1984; Kennicutt *et al.* 1995). The restructuring of cool gas will in turn influence the collapse of molecular clouds and attendant star formation (*e.g.*, McCray & Kafatos 1987). Likewise, the hot ionized medium (HIM) is believed to originate within these superbubbles and Type Ia supernova remnants (SNRs), hence the evolution of these structures determines whether and how this gas is released into the general ISM. Models for the ISM are strongly dependent on whether the coronal gas is the pervasive, dominant component, as envisioned by *e.g.*, McKee & Ostriker (1977), or whether it plays a lesser role as favored by *e.g.*, Slavin & Cox (1993), returning to a paradigm closer to the two-phase ISM of Field, Goldsmith, & Habing (1969).

The standard model for understanding the evolution of superbubbles and other shell structures is that of an adiabatic, pressure-driven bubble, with continuous wind energy injection (*e.g.*, Weaver *et al.* 1977; Dyson 1977; Pikel’ner 1968). It has generally been assumed that in later stages, successive supernovae (SNe) can be treated as an approximate continuous energy injection, and are able to power the growth of supergiant shells (*e.g.*, Mac Low & McCray 1988). Such supergiant shells, having radii of hundreds of pc, could then blow out of the galactic disk, releasing hot gas into the halo, possibly in a galactic fountain cycle.

However, recent evidence suggests that superbubble evolution is often not as simple as described by the standard model. Many superbubbles exhibit expansion velocities that are too high to be consistent with the standard evolution, and a correlation of bright X-ray emission with many of these objects suggests acceleration by SNR impacts (Oey 1996). In such cases, not all the available SN energy will be thermalized to power the shell expansion, thus the detailed effect that discrete SNe have on the long-term shell evolution remains unclear. Likewise, there is evidence that the growth rate of the shells may be overestimated, perhaps owing to an overestimate in input wind power predicted by assumed stellar mass-loss rates (Oey 1996; García-Segura & Mac Low 1995; Drissen *et al.* 1995). Therefore much remains unclear about the details of superbubble evolution.

A demonstrative example is the superbubble DEM 152 (N44) in the Large Magellanic Cloud. *ROSAT* observations of this object clearly show hot gas escaping through a “blowout” feature (Magnier *et al.* 1996), and this object also exhibits kinematics discrepant from the standard model (Oey & Massey 1995). If the ISM has low-density channels that encroach upon the superbubble environment, such evolutionary disruptions could signal a significant release of hot gas into the surroundings, and not necessarily out of the plane of galactic disks. The details of superbubble evolution thus have a direct consequence for the relative volumes of coronal gas in galactic disks and halos. Examples such as DEM 152 demonstrate the uncertainties in our understanding of superbubble evolution, and the importance to the global ISM.

One approach to test the assumed evolution is an examination of the superbubble size distribution in galaxies. This can be predicted from the evolutionary model in combination with a given production rate and mechanical luminosity function. A subsequent comparison with observed size distributions can then yield insight on the evolutionary assumptions and possible consequences for the inferred structure of the ISM. The cumulative size distribution of radiative SNRs has long been used as a diagnostic of SN parameters (*e.g.*, Hughes, Helfand, & Kahn 1984), but it can also be used to test evolutionary models for SNRs and superbubbles. An earlier investigation with a foray into this technique was carried out for SNRs by Cioffi & Shull (1991), who pointed out that the differential size distribution is a much more powerful diagnostic than the cumulative size distribution. In this work, we present a prediction for the differential size distribution for superbubbles and compare the results with HI observations of nearby galaxies. We will then examine the results with regard to the structure and porosity of the ISM.

We will consider a rather rudimentary model for superbubble evolution, with the aim of identifying dominant effects, rather than precisely reproducing observations. For example, the size distribution of Sedov-Taylor SNRs is predicted to increase as $N(R) \propto R^{5/2}$ (Hughes *et al.* 1984), for uniform ISM and stellar properties, whereas HI hole distributions in galaxies all show size distributions that decrease with shell radius R . Our objective is to derive gross general properties that would be expected as a result of the simplest practical application of the standard model. Agreements and disagreements with observations will then be instructive in understanding the features of the model that dominate the resultant size distribution and shell evolution, with attendant consequences for the structure of the ISM.

The paper is organized as follows. In §2, we work out general expressions for the assumed shell evolution and derived size distributions, for three combinations of shell creation and mechanical power input: (a) continuous creation, single luminosity; (b) single burst, luminosity spectrum; and (c) continuous creation, luminosity spectrum. In §3, we evaluate each of the solutions for the standard, adiabatic shell evolution. We also briefly examine the standard, momentum-conserving evolution. To obtain the slope of the mechanical luminosity spectrum, we examine evolutionary effects in the H II region luminosity function in §4. In §5, we compare our predictions with HI observations in four nearby galaxies, with attention to the slope, normalization, and peak of the size distributions. We also estimate supernova rates based on our analysis. The consequences are discussed in §6, where we examine the regimes of applicability for our predictions. Here we discuss the role of processes likely to modify the size distributions, and the role of alternate shell creation mechanisms. These effects are likely to be dependent on galaxy type. We also derive expressions for the ISM porosities resulting from our analysis, and compute porosities for the four nearby galaxies and the Milky Way. Our results are summarized in §7.

2 GENERAL ANALYTIC EXPRESSIONS

2.1 Assumptions

Superbubble expansion is presumed to be powered by the stellar winds, and especially, SNe of the parent OB association. It has been customary to represent the SN power as a continuous energy injection analogous to a wind (*e.g.*, Mac Low & McCray 1988), in which over half the SN energy is thermalized to drive the shell expansion. We will adopt this standard, adiabatic representation (*e.g.*, Weaver *et al.* 1977; Dyson 1977). For the purpose of comparing with HI “hole” data and ISM porosities, we are particularly interested in the superbubble cavity, which in this thin-shell approximation is considered to evolve identically to the outer radius. We also assume that the mechanical luminosity $L(t)$, dominated by the SNe, remains constant as a function of time t . As shown by Shull & Saken (1995), this is a reasonable approximation for realistic slopes of the stellar initial mass function (IMF). This constant $L(t)$ is then assumed to continue until the lowest-mass SN progenitors expire at $t = t_e$, which corresponds to a stellar mass of about $8 M_\odot$, or a period of roughly $t_e = 40$ Myr. A variation in input power may occur in the initial stages ($\lesssim 3 - 4$ Myr) while L is dominated by the stellar wind phase (*e.g.*, Shull & Saken 1995), but this stage is short relative to t_e , the total period of energy input. Leitherer & Heckman (1995) and Ferrière (1995) show that a starburst over this period does not substantially alter this approximation. A uniform ambient medium is assumed throughout, although in §6 we will discuss effects expected from disk galaxy gas distributions.

As will become apparent below, the endstage of shell evolution is vitally important to this analysis, but is fraught with uncertainties. We will consider the following simple model, keeping in mind our motivation of testing the simplest-case standard evolution. In most cases, eventually the superbubbles’ internal pressure $P_i \lesssim P_0$, the ambient pressure of the interstellar medium, while still at ages $t < t_e$. We will consider that for such objects, the superbubble growth stalls when $P_i = P_0$. At this stage, radiative losses are thought to become important, confining the shell growth. Simulations by García-Segura & Franco (1996), for example, show that the growth of the cavity radius does stall at times close to the sonic point. We will assume that the superbubbles survive at the stall radius R_f until the input power stops at time t_e . In principle, the shells will begin to disintegrate, owing to ambient random motions. However, the disintegration timescale may be fairly long; for example, it is $R_f/v_{\text{rms}} = 10$ Myr for ambient rms velocity $v_{\text{rms}} = 5 \text{ km s}^{-1}$ and $R_f = 50$ pc. Furthermore, the process of disintegration will still leave detectable cavities, so it is unclear how this effect can be quantified. We note that if the breakup of objects into smaller subunits occurs such that the ratio of subunit sizes is universal for all objects, then a power law size distribution remains unaffected (Clarke 1996). Our analysis will therefore not consider elimination of shells at ages $t < t_e$, nor differential elimination among the shell population. Finally, an important feature regarding stalling is the existence of a monotonic correspondence between L and R_f , for a uniform ISM.

Objects that never achieve pressure equilibrium with the ISM are simply assumed to grow until t_e . Finally, all objects are assumed to survive for an additional nominal period $t_s \ll t_e$, which is the same for all shells.

Within individual clusters, we take the star formation to occur in a single, instantaneous burst. Massey *et al.* (1995a, b) find that in general the duration of star formation is $\lesssim 3$ Myr for associations in the Magellanic Clouds and the Galaxy, which again is short relative to t_e . The spectrum of associated mechanical luminosities is a critical parameter; we will consider both a single, global value for L , and a power-law luminosity function (LF):

$$\frac{dN}{dL} = \phi(L) = AL^{-\beta} \quad , \quad (1)$$

normalized such that $\int \phi(L) dL = 1$. In §4 we will discuss the form of $\phi(L)$, and in particular, the value of β ; our analysis of $\phi(L)$ will assume the stellar IMF to be constant. We will also consider a constant cluster formation rate $\psi(t)$, and an instantaneous burst of cluster formation.

We first present the general expressions for the superbubble size distribution in the case that the shells grow according to the generic law:

$$R = \min\left(R(L, t), R_f(L)\right) \quad . \quad (2)$$

where $R_f(L)$ is the radius at which a superbubble stalls, which is dependent only on the input L , for uniform ISM parameters. We now consider the production of superbubbles for the simple cases of luminosity distribution $\phi(L)$ and formation rate $\psi(t)$ mentioned above, with respect to the stalling and continuous-growth evolutionary schemes. In each case, we derive $N(R)$, defined such that the number of superbubbles with radii in the range R to $R + dR$ is $N(R) dR$.

2.2 Continuous Creation, Single Luminosity

If superbubbles are generated at a constant rate ψ , then the number of growing shells with radii in the range R to $R + dR$ is equal to ψdt where dt is the time interval for creation corresponding to this radial range. Thus, the differential size distribution is,

$$N_{\text{grow}}(R) = \psi \left(\frac{\partial R}{\partial t} \right)^{-1} . \quad (3)$$

[Note that partial derivatives with respect to t and L are evaluated at constant L and t respectively.]

Recalling the correspondence between L and stall radius R_f , the single-valued $\phi(L) = L_0$ will therefore yield a single-valued $N_{\text{stall}} \equiv N(R_f)$ for stalled objects:

$$N_{\text{stall}}(R) = \psi \left(t_e - t_f(L_0) \right) \cdot \delta \left(R - R_f(L_0) \right) , \quad (4)$$

where $t_f(L_0)$ is the age at which a shell powered by L_0 stalls.

2.3 Single Burst, Luminosity Spectrum

If N_b superbubbles are created in an instantaneous burst, then after time t , the number of growing objects with radii in the range R to $R + dR$ is equal to $N_b \phi(L) dL$, where L and dL are the luminosity and range corresponding to this interval in R . Thus,

$$N_{\text{grow}}(R) = N_b \phi(L) \left(\frac{\partial R}{\partial L} \right)^{-1} . \quad (5)$$

Similarly, the distribution of stalled shells is given by:

$$N_{\text{stall}}(R) = N_b \phi(L) \left(\frac{\partial R_f}{\partial L} \right)^{-1} , \quad (6)$$

2.4 Continuous Creation, Luminosity Spectrum

2.4.1 Growing Shells

The form of $N(R)$ in this case can be obtained from the generalisation of either equation 3 or 5. In the former case, $N(R)$ is obtained by integrating equation 3 over the luminosity distribution:

$$N_{\text{grow}}(R) = \int_{L_l}^{L_u} \psi \phi(L) \left(\frac{\partial R}{\partial t} \right)^{-1} dL , \quad (7)$$

whilst in the latter case $N(R)$ is obtained by integrating equation 5 over a continuous creation rate:

$$N_{\text{grow}}(R) = \int_{t_l}^{t_u} \psi \phi(L) \left(\frac{\partial R}{\partial L} \right)^{-1} dt . \quad (8)$$

Equations 7 and 8 are equivalent in this situation, provided the limits of integration are correctly chosen. Note that these limits are functions of R , determined by the limiting conditions required to produce a given R . For a luminosity distribution truncated at L_{min} and L_{max} , the lower limit of integration for equation 7 is

$$L_l = \min \left(L(R, t_e), L_f(R) \right) , \quad L_l \geq L_{\text{min}} . \quad (9)$$

Here, $L(R, t_e)$ represents the luminosity for which the shell attains the given radius R within the maximum allowable time, t_e , whereas $L_f(R)$ is the luminosity such that a shell of luminosity L_f stalls at R , i.e., $R_f(L_f) = R$. Likewise, the upper limit of integration is

$$L_u = L_{\text{max}} , \quad (10)$$

representing the luminosity of the youngest shells that have grown to radius R . In the same vein, the lower limit of integration for equation 8 is

$$t_l = t(R, L_{\text{max}}) , \quad (11)$$

implying that no shells contribute to $N(R)$ if they were formed so recently that even the most luminous have not yet grown to R . Likewise, the upper limit is

$$t_u = \min \left(t_f(L), t(R, L_{\text{min}}) \right) , \quad t \leq t_e . \quad (12)$$

For the case of continuous growth with no possibility of stalling, the most distant epoch contributing to $N(R)$ is determined only by L_{\min} . Thus in that case $t_u = t(R, L_{\min})$, as long as this is shorter than t_e . If, however, the possibility of stalling is included, then the contribution from growing shells is additionally limited to periods shorter than $t_f(R, L)$, where t_f is the age at which a shell stalls at radius R (see equation 2).

2.4.2 Stalled Shells

By analogy to equation 8, the stalled shells are described by,

$$N_{\text{stall}}(R) = \int_{t_l}^{t_u} \psi \phi(L) \left(\frac{\partial R_f}{\partial L} \right)^{-1} dt \quad , \quad (13)$$

with $t_l = t_f(R)$, and $t_u = t_e$, where $t_f < t_e$.

2.4.3 Surviving Shells

In this section, we also include the possibility of a survival phase (§2.1) beyond t_e , of duration t_s . For shells stalling at $t_f < t_e$:

$$N_{\text{sur}}(R) = \int_{t_e}^{t_e+t_s} \psi dt \phi(L) \left(\frac{\partial R_f}{\partial L} \right)^{-1} \quad , \quad (14)$$

while for those that continue growing until t_e , therefore having $t_f > t_e$:

$$N_{\text{sur}}(R) = \int_{t_e}^{t_e+t_s} \psi dt \phi(L) \left(\frac{\partial R}{\partial L} \right)^{-1} \quad . \quad (15)$$

These yield,

$$N_{\text{sur}}(R) = \psi t_s \phi(L) \left(\frac{\partial R_f}{\partial L} \right)^{-1} \quad (16)$$

and

$$N_{\text{sur}}(R) = \psi t_s \phi(L) \left(\frac{\partial R}{\partial L} \right)^{-1} \quad . \quad (17)$$

2.4.4 Total Size Distributions

The complete shell evolution is summarized by

$$R(L, t) = \left\{ \begin{array}{ll} R(L, t) \quad , & t < t_f(L) \quad , \quad t_f(L) < t_e \\ R_f(L) \quad , & t_f(L) < t < t_e + t_s \quad , \quad t_f(L) < t_e \\ R(L, t_e) \quad , & t_e < t < t_e + t_s \quad , \quad t_f(L) > t_e \end{array} \right\} \quad . \quad (18)$$

As mentioned above, any given L uniquely determines corresponding stall parameters $R_f(L)$ and $t_f(L)$. Applying this relation to t_e , we denote the stall parameters corresponding to t_e as R_e and L_e . In other words, a superbubble with input power L_e would just stall at radius R_e and age t_e . Since the input power ceases at this time, t_e is the maximum possible stalling age. Thus shells larger than R_e are all either growing or in the survival stage, because their $t_f > t_e$. Conversely, the population of shells smaller than R_e contains a combination of growing, stalled, and surviving objects.

Therefore, for $R < R_e$, the total distribution is given by,

$$N(R) = N_{\text{grow}}(R) + N_{\text{stall}}(R) + N_{\text{sur}}(R) \quad . \quad (19)$$

For the case $L_{\min} < L(R, t_e)$ and $L_{\max} \rightarrow \infty$, the contribution to $N(R)$ from growing superbubbles is given by equation 8:

$$N_{\text{grow}}(R) = \int_0^{t_f(R)} \psi \phi(L) \left(\frac{\partial R}{\partial L} \right)^{-1} dt \quad , \quad (20)$$

whilst the contribution from stalled systems is given by equation 13:

$$N_{\text{stall}}(R) = \psi \cdot (t_e - t_f(R)) \phi(L) \left(\frac{\partial R_f}{\partial L} \right)^{-1} . \quad (21)$$

The distribution for surviving shells, $N_{\text{sur}}(R)$, is given by equation 16.

For $R > R_e$, the total size distribution is,

$$N(R) = N_{\text{grow}}(R) + N_{\text{sur}}(R) . \quad (22)$$

For the contribution due to growing superbubbles, equation 8 is now written:

$$N_{\text{grow}}(R) = \int_0^{t_e} \psi \phi(L) \left(\frac{\partial R}{\partial L} \right)^{-1} dt , \quad (23)$$

again for $L_{\text{min}} < L(R, t_e)$ and $L_{\text{max}} \rightarrow \infty$. Likewise, the shells in the survival phase are, by assumption, preserved at their instantaneous radii at time t_e , so that $N_{\text{sur}}(R)$ is given by equation 17.

3 EXPRESSIONS SPECIFIC TO THE STANDARD EVOLUTION

We now incorporate the standard evolution for adiabatic, pressure-driven superbubbles to the expressions developed above. The growth of the shell radius is described by (*e.g.*, Weaver *et al.* 1977):

$$R = \left(\frac{250}{308\pi} \right)^{1/5} L^{1/5} \rho^{-1/5} t^{3/5} , \quad (24)$$

where ρ is the mass density of a uniform ambient medium, and all units are cgs. The corresponding evolution of the interior pressure is

$$P_i = \frac{7}{(3850\pi)^{2/5}} L^{2/5} \rho^{3/5} t^{-4/5} . \quad (25)$$

In what follows, it is convenient to use R_e , t_e , and L_e as scaling parameters, recalling that R_e and L_e correspond to the stall criterion at the characteristic time t_e . Equations 24 and 25 can now be written,

$$\frac{R}{R_e} = \left(\frac{L}{L_e} \right)^{1/5} \left(\frac{t}{t_e} \right)^{3/5} , \quad (26)$$

$$\frac{P_i}{P_0} = \left(\frac{L}{L_e} \right)^{2/5} \left(\frac{t}{t_e} \right)^{-4/5} . \quad (27)$$

As discussed previously, we consider that the shell growth stalls when $P_i = P_0$, the ambient pressure. This condition therefore implies a stall age:

$$\frac{t_f}{t_e} = \left(\frac{L}{L_e} \right)^{1/2} , \quad (28)$$

Thus, by equation 26,

$$\frac{R_f}{R_e} = \left(\frac{L}{L_e} \right)^{1/2} . \quad (29)$$

Equations 28 and 29 demonstrate the correspondence between stalling age t_f and radius R_f for a given input power L . The corresponding relation between t_f and R_f is,

$$\frac{t_f}{t_e} = \frac{R_f}{R_e} . \quad (30)$$

Thus the final age t_f is directly proportional to the final radius R_f .

For a given t_e , equations 24 and 25 give:

$$R_e = \frac{5}{7^{1/2}} \left(\mu m_{\text{H}} \right)^{-1/2} n^{-1/2} P_0^{1/2} t_e \quad (31)$$

$$L_e = \frac{550\pi}{7^{3/2}} \left(\mu m_{\text{H}} \right)^{-3/2} n^{-3/2} P_0^{5/2} t_e^2 , \quad (32)$$

in cgs units, where n is the number density of the uniform ambient medium and μ is the mean particle weight. Note that equations 31 and 32 are applicable in general for the relation between R_f , t_f , and L_f as well. For ISM parameters $n = 0.5 \text{ cm}^{-3}$, $\mu = 1.25$, and $P_0 = 3 \times 10^{-12} \text{ dyne cm}^{-2}$, the characteristic time $t_e = 40 \text{ Myr}$ implies $R_e = 1300 \text{ pc}$ and $L_e = 2.2 \times 10^{39} \text{ erg s}^{-1}$.

3.1 Continuous Creation, Single Luminosity

As described in §2.2, the growing shells are the interesting case here, for which equations 3 and 26 imply,

$$N_{\text{grow}}(R) = \frac{5}{3} \psi \frac{t_e}{R_e} \left(\frac{L_0}{L_e} \right)^{-1/3} \left(\frac{R}{R_e} \right)^{2/3}. \quad (33)$$

Thus for a single-valued LF of luminosity L_0 , the size distribution is an increasing function of $R^{2/3}$, which results from the slower growth of large shells. As the stalled shells accumulate, they also superimpose a δ -function at $R_f(L_0)$, described by equation 4.

3.2 Single Burst, Luminosity Spectrum

Here we assume that $\phi(L)$ is a power law as given by equation 1. For the growing shells with age $t < t_e$, equations 5 and 26 yield,

$$N_{\text{grow}}(R) = 5AN_b(1 - F_{\text{st}}) \frac{L_e^{1-\beta}}{R_e} \left(\frac{R}{R_e} \right)^{4-5\beta} \left(\frac{t}{t_e} \right)^{-3+3\beta}, \quad (34)$$

where $1 - F_{\text{st}}$ is the fraction of N_b corresponding to growing shells. The fraction of stalled shells is given by,

$$F_{\text{st}} = \int_{L_{\text{min}}}^L AL^{-\beta} dL, \quad (35)$$

where L is the luminosity corresponding to the largest stalled shells. As we shall see in §5, realistic values of the LF index fall in the range $1 \lesssim \beta \lesssim 3$, for which $N(R) \propto R^{4-5\beta}$ would be an inverse power law in R . This results from the larger fraction of small, weak- L shells.

The stalled shells are described by equation 6. Together with equation 29, this gives,

$$N_{\text{stall}}(R) = 2AN_b F_{\text{st}} \frac{L_e^{1-\beta}}{R_e} \left(\frac{R}{R_e} \right)^{1-2\beta}. \quad (36)$$

The total size distribution at times before all the objects have stalled and $R < R_e$ would be the sum of equations 34 and 36. Owing to the large numbers of weak- L objects, equation 36 will normally dominate $N(R)$ in relative numbers. However, these stalled shells will only be present out to radius $R_f(t_b)$ corresponding to the age t_b of the burst. At this radius, there will be a discontinuous jump by a factor of $\frac{5}{2}$, resulting from the different coefficients of $\frac{\partial R}{\partial L}$ (cf. equation 26) and $\frac{\partial R_f}{\partial L}$ (cf. equation 29). The subset of objects with $R > R_e$ will not stall in $t < t_e$ and will therefore follow the relation given by equation 34.

3.3 Continuous Creation, Luminosity Spectrum

3.3.1 $R < R_e$

We shall now evaluate the expressions in §2.4.4, for the population of shells with radii $R < R_e$, incorporating $\phi(L)$ as given by equation 1. For $\beta > \frac{2}{3}$, $L_{\text{min}} < L(R, t_e)$, and $L_{\text{max}} \rightarrow \infty$, the size distribution for the growing shells is given by equation 20. With the aid of equation 26 this yields,

$$N_{\text{grow}}(R) = 5A\psi \frac{L_e^{1-\beta}}{R_e} \frac{t_e}{-2+3\beta} \left(\frac{R}{R_e} \right)^{4-5\beta} \left(\frac{t_f}{t_e} \right)^{-2+3\beta}. \quad (37)$$

For each R we are summing over all ages up to t_f that yield a stall radius R , so that (from equation 30) equation 37 becomes,

$$N_{\text{grow}}(R) = 5A\psi \frac{L_e^{1-\beta}}{R_e} \frac{t_e}{-2+3\beta} \left(\frac{R}{R_e} \right)^{2-2\beta}. \quad (38)$$

In the case that $\beta < \frac{2}{3}$, equation 8 is dominated by t_l (equation 11), and if $L_{\text{min}} > L(R, t_e)$, then $t_u = t(R, L_{\text{min}})$. For both of these cases,

$$N_{\text{grow}}(R) = 5A\psi \frac{L_e^{1-\beta}}{R_e} \left(\frac{L_{\text{max}}}{L_e}\right)^{\frac{2}{3}-\beta} \frac{-t_e}{-2+3\beta} \left(\frac{R}{R_e}\right)^{2/3}. \quad (39)$$

Thus for $L_{\text{min}} \neq 0$, the slope of the size distribution turns over from $4 - 5\beta$ in equation 37 to a positive slope of $\frac{2}{3}$, at $R < R(L_{\text{min}}, t_e)$, where $R(L_{\text{min}}, t_e)$ corresponds to the case in the absence of stalling. Beware that the resulting peak in $N_{\text{grow}}(R)$ does not correspond to the maximum peak in the total $N(R)$, since the latter is dominated by stalled shells, as we shall see below.

For the stalled shells, equations 21 and 29 yield,

$$N_{\text{stall}}(R) = 2A\psi \frac{L_e^{1-\beta}}{R_e} t_e \left(\frac{R}{R_e}\right)^{1-2\beta} \left(1 - \frac{R}{R_e}\right). \quad (40)$$

Note that for these stalled objects, the term $\left(1 - \frac{R}{R_e}\right) = \left(1 - \frac{t_f}{t_e}\right)$ by equation 30. This therefore represents the fraction of their lifetime t_e that is spent in the stalled state, for shells of radius R . Although multiplying out equation 40 yields two terms with dependences $R^{1-2\beta}$ and $R^{2-2\beta}$, $N_{\text{stall}}(R)$ is dominated by $R^{1-2\beta}$ since we are in the regime $\frac{R}{R_e} < 1$. This is the same dependence as the stalled objects in equation 36.

The shells in the survival phase are given by equation 16, which becomes

$$N_{\text{sur}}(R) = 2A\psi \frac{L_e^{1-\beta}}{R_e} t_s \left(\frac{R}{R_e}\right)^{1-2\beta}. \quad (41)$$

Again this is similar to equation 36, since this case is equivalent to the distribution resulting from a single burst containing ψt_s objects.

Adding together equations 38, 40, and 41, the total size distribution for superbubbles with $R < R_e$ and $\beta > \frac{2}{3}$ is:

$$N(R) = A\psi \frac{L_e^{1-\beta}}{R_e} \left(\frac{R}{R_e}\right)^{1-2\beta} \left[2(t_e + t_s) + \frac{9-6\beta}{-2+3\beta} t_e \left(\frac{R}{R_e}\right) \right]. \quad (42)$$

3.3.2 $R > R_e$

For shells larger than the characteristic radius R_e , the distribution of growing objects is given by equation 23. This is identical to equation 20, except that the integration is over the range $(0, t_e)$ rather than $(0, t_f(L))$. For $\beta > \frac{2}{3}$, equation 23 therefore yields,

$$N_{\text{grow}}(R) = 5A\psi \frac{L_e^{1-\beta}}{R_e} \frac{t_e}{-2+3\beta} \left(\frac{R}{R_e}\right)^{4-5\beta}. \quad (43)$$

Note that the R dependence of $N_{\text{grow}}(R)$ in equation 43 is different from that of shells that grow with the possibility of stalling (equation 38). This is due to the fact that the upper limit of integration in equation 8 is a function of R only when the possibility of stalling is included.

The shells in the survival stage are described by equation 17, yielding,

$$N_{\text{sur}}(R) = 5A\psi \frac{L_e^{1-\beta}}{R_e} t_s \left(\frac{R}{R_e}\right)^{4-5\beta}. \quad (44)$$

Adding together equations 43 and 44, the overall size distribution for supergiant shells with $R > R_e$ and $\beta > \frac{2}{3}$ is:

$$N(R) = 5A\psi \frac{L_e^{1-\beta}}{R_e} \left(\frac{R}{R_e}\right)^{4-5\beta} \left[\frac{t_e}{-2+3\beta} + t_s \right]. \quad (45)$$

This again exhibits the $R^{4-5\beta}$ dependence as seen in equation 34, which describes the distribution for freely growing shells. This reflects the fact that objects in this size range will never attain the stalling criterion. In general, this relation is a very steep function of R compared to equation 42 for $R < R_e$. The criterion $R > R_e$ corresponds to $L > L_e$, which may provide a convenient defining criterion for these larger-scale phenomena, for example, starburst events. There might possibly be applications for equation 45 for a large sample of starburst phenomena with uniform properties.

In the case that $\beta < \frac{2}{3}$, equation 8 is dominated by the lower limit t_l , as in the regime for $R < R_e$. $N_{\text{grow}}(R)$ in that case is therefore given by equation 39. Note that, for $t_s > 0$, $N(R)$ is *not* continuous at $R = R_e$. This is a consequence of the change in slope of the $L - R$ relation for shells surviving at R_e , as is apparent from equations 26 and 29 (see §2.4.3).

3.4 Robustness of the Result

The dependence $N(R) \propto R^{1-2\beta}$ appears to be a fairly robust description, since stalled superbubbles quickly dominate most situations for both constant and instantaneous superbubble formation. In addition, we also mentioned above that the slope will not change if the breakup of shells into subunits is independent of the original size (Clarke 1996).

Furthermore, the $R^{1-2\beta}$ dependence turns out not to be unique to the standard evolution. Consider the general relation,

$$\left(\frac{R}{R_e}\right) = \left(\frac{L}{L_e}\right)^x \left(\frac{t}{t_e}\right)^y. \quad (46)$$

Within factors of unity, the stalling criterion is equivalent to setting the shell ram pressure $\rho_s v^2 \sim P_0$, where ρ_s is the shell density and v is the shell expansion velocity. Therefore, this is the same as requiring that v stall at a limiting velocity v_0 associated with P_0 of the ambient medium. We have,

$$v = \frac{dR}{dt} = y \frac{R_e}{t_e} \left(\frac{L}{L_e}\right)^x \left(\frac{t}{t_e}\right)^{y-1}. \quad (47)$$

Setting this equal to v_0 , we obtain,

$$\frac{t_f}{t_e} = \left(\frac{v_0}{y} \cdot \frac{t_e}{R_e}\right)^{\frac{1}{y-1}} \left(\frac{L}{L_e}\right)^{\frac{x}{1-y}}, \quad (48)$$

which is the generalization of equation 28. Note that R_e is defined such that $\frac{v_0}{y} \cdot \frac{t_e}{R_e} = 1$. With equation 46, we then have,

$$\frac{t_f}{t_e} = \frac{y}{v_0} \cdot \frac{R_e}{t_e} \left(\frac{R_f}{R_e}\right), \quad (49)$$

analogous to equation 30. The relation $t_f \propto R_f$ therefore applies generally to any growth law described by equation 46. In the standard adiabatic model, $x = \frac{1}{5}$ and $y = \frac{3}{5}$, yielding $t_f \propto L^{1/2}$. Other values of x and y yielding $\frac{x}{1-y} = \frac{1}{2}$ will also produce equations 28 – 30, and therefore our previous expressions for $N_{\text{stall}}(R)$ (equation 40) and $N_{\text{sur}}(R)$ (equation 41) would still be valid.

3.4.1 Momentum-Conserving Evolution

It turns out that the non-adiabatic, momentum-conserving shell evolution described by Steigman, Strittmatter, & Williams (1975) fulfills this condition. The momentum-conserving growth is given by,

$$\left(\frac{R}{R_e}\right) = \left(\frac{L}{L_e}\right)^{1/4} \left(\frac{t}{t_e}\right)^{1/2}, \quad (50)$$

Therefore, the only component of $N(R)$ that differs from the adiabatic case is that for $N_{\text{grow}}(R)$, for which equations 20 and 50 give:

$$N_{\text{grow}}(R) = 4A\psi \frac{L_e^{1-\beta} t_e}{R_e} \frac{1}{-1+2\beta} \left(\frac{R}{R_e}\right)^{2-2\beta}, \quad (51)$$

in contrast to equation 38. The total size distribution for the momentum-conserving evolution in the regime $R < R_e$, $\beta > \frac{1}{2}$ is therefore,

$$N(R) = A\psi \frac{L_e^{1-\beta}}{R_e} \left(\frac{R}{R_e}\right)^{1-2\beta} \left[2(t_e + t_s) + \frac{6-4\beta}{-1+2\beta} t_e \left(\frac{R}{R_e}\right) \right], \quad (52)$$

which may be compared to equation 42. $N(R)$ in this case (equation 52) is still dominated by the term having $R^{1-2\beta}$ dependence.

To check whether typical observed superbubbles are still in the regime $R < R_e$ for this case, we need to compute the new value of R_e , again for $t_e = 40$ Myr. The unscaled relations for the radius and interior pressure are:

$$R = \left(\frac{3L}{\pi\rho v_\infty}\right)^{1/4} t^{1/2} \quad (53)$$

$$P_i = \frac{\dot{M}v_\infty}{4\pi R^2}, \quad (54)$$

where \dot{M} and v_∞ are the mass-loss rate and velocity of the “wind,” thereby giving $L = \frac{1}{2}\dot{M}v_\infty^2$. The pressure equilibrium stalling criterion now yields,

$$R_e = 6^{1/2} \left(\mu m_{\text{H}} \right)^{-1/2} n^{-1/2} P_0^{1/2} t_e \quad . \quad (55)$$

The dependences are the same as equation 31, but with a coefficient of $6^{1/2}$ in the momentum-conserving case versus $5/7^{1/2}$ in the adiabatic case. Thus, for a given stall age t_f , the corresponding stall radius of a momentum-conserving superbubble will be larger than that of an adiabatic superbubble. This results from the fact that the same value of t_f corresponds to a larger value of L in the momentum-conserving case because more energy is needed to maintain growth during the entire period t_f . Therefore the final stall radius R_f for the momentum-conserving evolution is larger than the adiabatic case for a given t_f . For the same default ISM parameters as the adiabatic case, equation 55 yields $R_e = 1700$ pc. Most observed superbubbles in galaxies indeed have radii smaller than this value. The form $N(R) \propto R^{1-2\beta}$ is therefore a fairly robust result for this simple representation of superbubble evolution.

4 DERIVING THE MECHANICAL LF FROM THE H II REGION LF

We must now consider the form of $\phi(L)$, the mechanical LF (MLF; equation 1), with regard to its slope β and the upper and lower limits. The MLF results from the stellar census present in the OB associations, which in turn manifests its presence through the H II region LF (H II LF). As recognized by Heiles (1990), the MLF and H II LF are closely linked. We will focus on clusters that are sufficiently rich so that statistical fluctuations in stellar membership have a negligible effect on the mean H α luminosity per star. We term such clusters “saturated,” and consider this limit for now, deferring a discussion of smaller, “unsaturated” clusters until §4.3.

For the saturated clusters, the total initial H α luminosity \mathcal{L}_0 , and the mechanical luminosity L , are both proportional to the total number of stars in the cluster, thus implying $L \propto \mathcal{L}_0$. Therefore, the slope of the MLF is equal to that of the H II LF. This is not, however, necessarily the same as the slope of the *observed* H II LF (von Hippel and Bothun 1990), because the H II region luminosity fades with time as the ionizing stars expire, and the observed H II LF contains objects of differing ages. Therefore, before we simply take the empirical slope of the H II LF as that of the MLF, we must first consider the possible effect of evolution on the H II LF. We will now examine this effect analytically.

4.1 Analytic Evolution of the H II Region LF

We characterise the evolution of the H II region luminosity by

$$\mathcal{L} = \mathcal{L}_0 f(t) \quad (56)$$

where $f(0) = 1$. We thus assume that the fractional fading in a given time, and hence the IMF, is the same for all clusters. Since the observed H II LFs are well described as power laws (*e.g.*, Kennicutt, Edgar, & Hodge 1989), we will presume the initial H II LF to have the same form:

$$\frac{dN_{\text{H}\alpha}}{d\mathcal{L}_0} \equiv \Phi(\mathcal{L}_0) = A_0 \mathcal{L}_0^{-\beta} \quad . \quad (57)$$

We adopt the index β as in the previous sections, because as argued above, we assume that $\phi(L)$ has the same exponent as $\Phi(\mathcal{L}_0)$. As with $\phi(L)$ (equation 1), $\Phi(\mathcal{L})$ is defined such that $\Phi(\mathcal{L}) d\mathcal{L}$ is the fraction of objects with H α luminosities in the range \mathcal{L} to $\mathcal{L} + d\mathcal{L}$. If the magnitude of $\frac{df}{dt}$ is large at early times, we would expect the steady-state observed H II LF to be steeper than the initial, since the brightest objects are quickly diminished. On the other hand, if f evolves strongly at late times, then the initial slope β is largely preserved.

The evolution of $\Phi(\mathcal{L})$ may be considered analogous to that of $N(R)$ (equation 7) above:

$$\Phi(\mathcal{L}) = \int_{\mathcal{L}}^{\mathcal{L}_{0,\text{up}}} \psi \Phi(\mathcal{L}_0) \left(-\frac{\partial \mathcal{L}}{\partial t} \right)^{-1} d\mathcal{L}_0 \quad , \quad (58)$$

where ψ is the constant cluster formation rate as before and the partial derivative with respect to t is evaluated at constant \mathcal{L} . The observed H II LF is determined by the contribution of objects at all ages to a given luminosity bin, and these therefore fall in the range $(\mathcal{L}, \mathcal{L}_{0,\text{up}})$. From equation 56,

$$\frac{\partial \mathcal{L}}{\partial t} = \mathcal{L}_0 \frac{df}{dt} \quad . \quad (59)$$

So in general,

$$\Phi(\mathcal{L}) = \int_{\mathcal{L}}^{\mathcal{L}_{0,\text{up}}} \psi \Phi(\mathcal{L}/f) \left(-\mathcal{L}_0 \frac{df}{dt} \right)^{-1} d\mathcal{L}_0 \quad (60)$$

where f and $\frac{df}{dt}$ are functions of \mathcal{L} and \mathcal{L}_0 as described by equation 56. The upper limit of integration is determined by the upper limit to the initial H II LF, $\mathcal{L}_{0,\text{up}}$. For a power law LF given by equation 57:

$$\Phi(\mathcal{L}) = -A_0 \mathcal{L}^{-\beta} \int_{\mathcal{L}/\mathcal{L}_{0,\text{up}}}^1 \psi(t) f^{\beta-1} \left(\frac{df}{dt} \right)^{-1} df \quad . \quad (61)$$

We now consider the form of $f(t)$. This depends on the stellar mass (m) vs. main-sequence lifetime (t_{ms}) relation, as well as the relative contributions to total \mathcal{L} from stars of different masses. Leitherer (1990, Figure 8) shows that fortuitously, for a standard Salpeter (1955) IMF, the contribution to \mathcal{L} from each unit mass bin $\frac{d\mathcal{L}}{dm}$, is approximately constant for all $m > 20 M_{\odot}$, while for lower-mass stars it plummets steeply.

As an exploratory case, we therefore make the approximation that only stars with $m \geq 20 M_{\odot}$ contribute to \mathcal{L} , and that the different masses contribute equally. We represent the $m - t_{\text{ms}}$ relation for $m \geq 20 M_{\odot}$ as a power law:

$$t_{\text{ms}} \propto m^{-d} \quad . \quad (62)$$

The Geneva stellar evolutionary models (Schaerer *et al.* 1993; Maeder 1990; Maeder & Meynet 1988) show that this relation actually increases somewhat faster than a simple power law, but for our purposes, the approximation is adequate. Fits to their models, which are the same as those used in Leitherer's (1990) study, yield $d \sim 0.65$ in the range $20 \leq m \leq 120 M_{\odot}$. If we furthermore assume that stars in each mass bin contribute a constant luminosity for the duration of their main sequence lifetimes and nothing thereafter, we then obtain the fading function,

$$f = \begin{cases} 1 \quad , & t < t_i \\ \frac{(t/t_{20})^{-1/d} - 1}{(t_i/t_{20})^{-1/d} - 1} \quad , & t \geq t_i \end{cases} \quad (63)$$

where $t_{20} \equiv t_{\text{ms}}(20 M_{\odot})$, and t_i is the time at which the \mathcal{L} fading begins, which is $t_{\text{ms}}(m_{\text{up}})$, where m_{up} is the upper-mass limit of the IMF. Applying equation 63 to equation 61, we obtain:

$$\Phi(\mathcal{L}) = A_0 \psi \mathcal{L}^{-a} \left[\int_{\mathcal{L}/\mathcal{L}_{0,\text{up}}}^1 \frac{\left(\frac{m_{\text{up}}}{m_{20}} - 1 \right) f^{\beta-1} t_{20} d}{\left[\left(\frac{m_{\text{up}}}{m_{20}} - 1 \right) f + 1 \right]^{d+1}} df + t_i \right] \quad , \quad (64)$$

using a to denote the slope of the observed H II LF, $\Phi(\mathcal{L}) \propto \mathcal{L}^{-a}$. The last term in equation 64 corresponds to shells with ages $t < t_i$, for which equation 61 diverges.

Equation 64 demonstrates that for $\beta > d + 1$, the integral is always dominated by its upper limit, so that ageing does not affect the form of the H II LF in this case. For $\beta < d + 1$, if $\frac{m_{\text{up}}}{m_{20}}$ is sufficiently large, then $\Phi(\mathcal{L})$ will asymptotically approach a slope of $d + 1$. Values for the observed slope are found to be $a \sim 2 \pm 0.5$ (*e.g.*, Kennicutt *et al.* 1989). Figure 1 shows the resultant $\Phi(\mathcal{L})$ from equation 64, numerically integrated for initial slopes β ranging from 0.5 to 2.5, with $d = 0.65$, $\mathcal{L}_{0,\text{up}} = 10^{40} \text{ erg s}^{-1}$, and $m_{\text{up}} = 120 M_{\odot}$. The curves are normalized to the same upper value to facilitate comparison. Each curve is labeled with the input value of β , which is within 4% of the resultant slope a , fitted over the region $\log \mathcal{L} < 36.5$. Thus it is apparent that evolution has essentially no effect on these slopes for $m_{\text{up}} = 120 M_{\odot}$. With the dashed line, we also show the result for $\beta = 1$, $d = 0.65$ and $m_{\text{up}} = 10^7 M_{\odot}$; this model confirms that the observed slope does tend to the asymptotic limit of $d + 1 = 1.65$ if m_{up} is sufficiently large, although this effect is clearly negligible for realistic situations.

Alternatively, we can estimate $f(t)$ directly from the population synthesis work of Leitherer & Heckman (1995). Figure 37 of that work shows the evolution of the total ionizing photon emission rate $S(\text{H}^0)$, and hence \mathcal{L} , for clusters with different IMFs and m_{up} . The fading function is relatively insensitive to these variables and is well approximated by a power law decrease with time, which does not drop to zero at t_{20} , but persists with the same power law at late times. From the Leitherer & Heckman (1995) standard model with a Salpeter IMF of slope 2.35 and $m_{\text{up}} = 100 M_{\odot}$, we fit a fading function slope $\eta = 5.0$ in the regime $\log(t/\text{Myr}) > 6.5$ and $\log(S(\text{H}^0)/\text{s}^{-1}) > 44$. This slope was also found by Beltrametti *et al.* (1982).

We thus parameterize the evolution as:

$$f = \begin{cases} 1 \quad , & t < t_i \\ (t/t_i)^{-\eta} \quad , & t \geq t_i \end{cases} \quad (65)$$

so that integration of equation 61 yields:

$$\Phi(\mathcal{L}) = \frac{\psi t_i A_0}{\eta(\beta - \frac{1}{\eta} - 1)} \mathcal{L}^{-\beta} \left[1 - \left(\frac{\mathcal{L}}{\mathcal{L}_{0,\text{up}}} \right)^{\beta - \frac{1}{\eta} - 1} \right] + \psi t_i A_0 \mathcal{L}^{-\beta} \quad . \quad (66)$$

This again implies that the slope of $\Phi(\mathcal{L})$ remains unaffected by ageing for $\beta > \frac{1}{\eta} + 1$, whereas if $\beta < \frac{1}{\eta} + 1$, ageing produces an observed slope $a = 1 + \frac{1}{\eta}$, independent of β and m_{up} . This minimum value of a reflects our argument above, that the

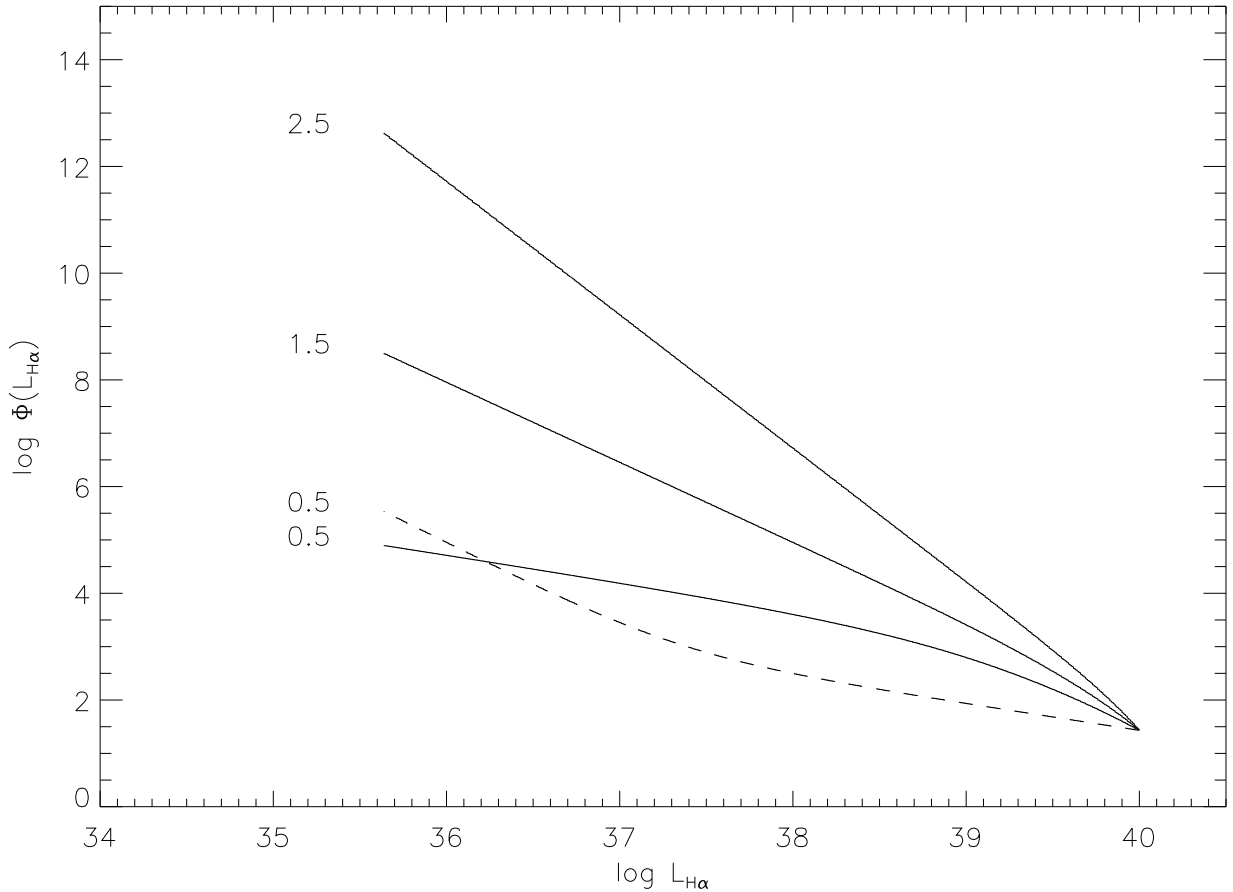


Figure 1. H II region LF resulting from the fading function given by equation 63, for $\log(\mathcal{L}_{\text{up}}/\text{erg s}^{-1}) = 40$, $d = 0.65$, and $m_{\text{up}} = 120 M_{\odot}$ (solid lines) and $m_{\text{up}} = 10^7 M_{\odot}$ (dashed line). The input values of β are shown for each model.

observed slope of $\Phi(\mathcal{L})$ is steepened if the nebular luminosity evolution is strong enough. Figure 2 demonstrates this behavior for $\eta = 5$ and a range of β , with the curves again normalized to the same value of $\mathcal{L}_{0,\text{up}}$. Thus if the slope of $\Phi(\mathcal{L}_0)$ is steep, intrinsically luminous systems are rare and therefore the faded remnants of such objects make a relatively small contribution to any bin of observed \mathcal{L} . Note that this steepening behavior in a was not apparent, for plausible values of m_{up} , in the case where $f(t)$ was set to 0 at time $t = t_{20}$ (equation 63). In that case, the dynamic range of the fading function $f(t)$ is small over most of the lifetime of an H II region. The stronger evolutionary effect resulting from equation 66 stems from the prolonged fading at late times in this prescription.

Note that η essentially corresponds to $1/d$ in the previous case. Recalling that d is the power law slope for the $m - t_{\text{ms}}$ relation (equation 62), a value of $\eta = 5.0$ suggests $d = 0.2$. This is considerably shallower than our previous estimate of 0.65, which was fitted from the model results of the Geneva group (*e.g.*, Maeder 1990), the same stellar models used by Leitherer & Heckman (1995). This would suggest that the luminosity evolution of the H II regions is affected by additional factors besides the turnoff of stars from the main-sequence, for example, spectral evolution of the stars while they are still in the H-burning phase. Clearer understanding of the behavior of $f(t)$ is needed to confirm the applicability of our analysis.

4.2 Discussion of Evolutionary Effects

We have shown how in principle ageing can cause the measured H II LF to be steeper than the initial, as cluster fading shifts an excess of objects into low luminosity bins. This effect is only manifest for flatter initial $\Phi(\mathcal{L}_0)$ with low β , where any bin of objects at given current luminosity \mathcal{L} contains an important contribution from initially luminous objects formed in the distant past. Thus for that case, it is the fading function $f(t)$ that determines the observed H II LF. Conversely, if the initial $\Phi(\mathcal{L}_0)$ is steep, then any bin of current luminosity is dominated by recently formed objects. In this case, ageing is unimportant, and

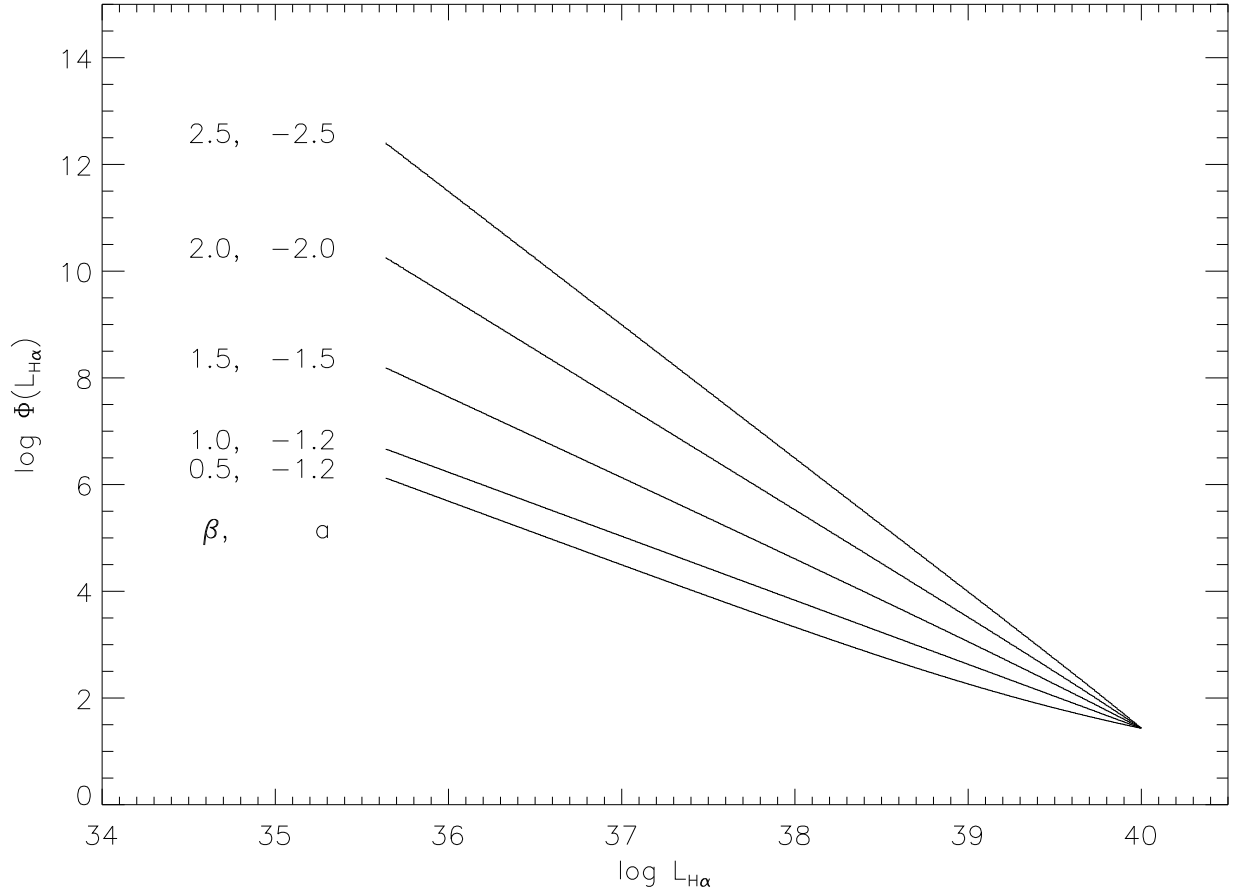


Figure 2. H II region LF resulting from the fading function given by equation 65, for $\log(\mathcal{L}/\text{erg s}^{-1}) = 40$, $\eta = 5.0$, and $m_{\text{up}} = 120 M_{\odot}$. The input values of β are shown for each model, along with the resulting slope a , fitted to the region $\log \mathcal{L} < 36.5$.

the observed $\Phi(\mathcal{L})$ has the same slope as the initial. Quantitatively, if the nebula fades according to a simple power law $t^{-\eta}$, then

$$a = \max\left(\beta, a_{\text{min}}\right), \quad a_{\text{min}} = 1 + \frac{1}{\eta} . \quad (67)$$

Thus for example, if $\eta = 1$, then measured values of $a = 2$ would imply only that $\beta \leq 2$. Hence, for any simple power-law $f(t)$ that does not steepen substantially at late times, there is a minimum value a_{min} , independent of β , given by equation 67. Therefore, if different galaxies have populations of H II regions characterised by different values of β , then this variety would be manifest only down to a limiting value set by the $f(t)$. An observed value of $a_{\text{min}} = \frac{1}{\eta} + 1$ can therefore be used to determine the actual slope η of the fading function. For example, $a_{\text{min}} = 1.4$ would imply an adjustment in the value of η from 5 to 2.5, which would require a much more gradual decline in H α luminosity for the H II regions than is predicted by the stellar models. However, η is extremely sensitive to the adopted value of a_{min} , so this test is unlikely to be practical in the near future. Furthermore, our ability to observe a_{min} depends on the actual existence of galaxies with H II LFs having initial $\beta < a_{\text{min}}$. At present the available data on H II LFs in different galaxies suggests $a \gtrsim 1.3 - 1.4$ (e.g., Banfi *et al.* 1993), but there are not yet enough data to evaluate whether there is a lower cutoff in the values of a . This is evidently an effect that can be sought in the future as H II LFs become available for a larger sample of galaxies.

We find, however, that this evolutionary effect of a minimum a is unlikely to be significant for observed H II LFs with spectral indices of $a \sim 2$, if we use $f(t)$ based on plausible population synthesis arguments. We have experimented with two prescriptions: one assuming an instantaneous cutoff in \mathcal{L} at $t > t_{20}$; and the other using continuous fading, $f(t) \propto t^{-\eta}$, based on population synthesis models by Leitherer and Heckman (1995). In each case, the power-law fading is too steep for the measured values of a to be explicable as an ageing effect, and thus we would conclude that a is a direct measure of β . We caution, however, that this result does depend on the assumed IMF and modeled stellar parameters that are used in the

Table 1. Observed Parameters

Galaxy	a	N_{HII}	HII Ref. ^a	N_{HI}	$h(\text{pc})$	HI Ref. ^a
SMC	1.9	93	(1)	501	(2000) ^b	(3)
Holm II	1.4	67	(2)	51	625	(4)
M31	2.1	207	(1)	140	120	(5)
M33	2.0	257	(1)	148	(100) ^b	(6)

^aReferences:

- (1) Kennicutt, Edgar, & Hodge (1989)
- (2) Hodge, Strobel, & Kennicutt (1994)
- (3) Staveley-Smith *et al.* (1996)
- (4) Puhe *et al.* (1992)
- (5) Brinks & Bajaja (1986)
- (6) Deul & den Hartog (1990)

^bValue for the SMC is based on Staveley-Smith's *et al.* (1996) estimate for the SMC HI morphology; value for M33 is assumed, not measured.

population synthesis models. Some of these parameters, for example, stellar ionizing fluxes (especially those contributed by B stars), are rather poorly known. Furthermore, this determination of β from a is based on stars with $m \gtrsim 20 M_{\odot}$, which is the population ionizing the HII regions. We are thereby assuming that the slope β extends to lower-mass stars, which dominate the MLF through their SNe. This is based on assumptions about the form of the IMF, and also the constancy of SN power for stars of different mass.

4.3 Unsaturated clusters

In the limit of small cluster membership number N_* , there is a wide dispersion in average H α contribution per star, according to the precise stellar membership of the cluster. As a result, a power law slope in the IMF produces a $\Phi(\mathcal{L}_0)$ of the same initial slope at high \mathcal{L}_0 , but which flattens at low \mathcal{L}_0 (McKee & Williams 1996). This is produced by the behavior of the scatter, due to small number statistics, in contributions to \mathcal{L}_0 from a bin of given N_* . These contributions scatter symmetrically on a linear scale of \mathcal{L}_0 , but logarithmically, they have a larger displacement to smaller values of $\log(\mathcal{L}_0)$, producing a consequent flattening of the luminosity spectrum. Monte Carlo simulations by McKee & Williams (1996) confirm that this flattening occurs at $\mathcal{L}_0 \sim \mathcal{L}_{m_{\text{up}}}$, the H α luminosity due to a single star of $m = m_{\text{up}}$. Clusters with $\mathcal{L}_0 < \mathcal{L}_{m_{\text{up}}}$ are not rich enough to saturate the IMF up to this maximum, and thus have varying mean H α contribution per star; whereas those with $\mathcal{L}_0 > \mathcal{L}_{m_{\text{up}}}$, again for a constant IMF, will have $\mathcal{L} \propto N_*$, and thereby a constant H α contribution per star. Note that we do not expect a similar turnover in the MLF because the relative contribution to L of each star is dominated by the SN power, which we assume to be independent of m . The correspondence between a and β therefore applies in the regime where both \mathcal{L}_0 and L scale with the number of stars in the associations.

For some galaxies, the slope of the HII LF shows a turnover to a shallower value at lower \mathcal{L} (*e.g.*, Kennicutt *et al.* 1989), which could possibly be due to this effect, with objects falling below cluster saturation. The value of $\mathcal{L}_{m_{\text{up}}}$, corresponding to the saturation turnover, is currently estimated at $\log \mathcal{L}_{m_{\text{up}}} \sim 38.0 - 38.5$ (Vacca *et al.* 1996; Panagia 1973). If the observed flattening of the HII LFs is caused by this effect, it is important to use the slope a derived from the upper end of the HII LF in estimating β . However, although the observed value of a might cause an underestimate of β when fitted over the entire range of \mathcal{L} , we will see below that, where the measured $N(R)$ is discrepant from that predicted, it requires *shallower* slopes in the MLF than those inferred from the HII LF.

5 COMPARISON WITH OBSERVATIONS

We can now compare the prediction with observations for individual galaxies that have been mapped in HI at sufficient resolution, and that have measured HII LFs. Table 1 lists observed parameters for nearby galaxies that we have examined. Values for the observed slope a of the HII LF, fitted from data in the listed reference, are given in Table 1, along with the total number of detected HII regions N_{HII} having $\mathcal{L} > 1 \times 10^{37} \text{ erg s}^{-1}$, and total number of detected HI holes N_{HI} . The limiting \mathcal{L} is that at which the surveys are complete for all the galaxies. We assume that all the HI holes correspond to superbubbles. Table 1 also lists the assumed HI scale height h , and reference for the HI mapping.

Table 2. Inferred Parameters

Galaxy	N_{tot}	$\psi(\text{Myr}^{-1})$	$\log A$	β^{a}	β_o^{b}	$\sigma(\beta_o)$	α_p^{c}	α_o
SMC	1.9×10^3	43	32.26	1.9	1.9	0.3	2.8	2.7
Holm II	1.4×10^3	31	13.98	1.4	1.6	1.2	1.8	2.1
M31	4.3×10^3	96	39.53	2.1	1.8	0.7	3.2	2.6
M33	5.4×10^3	120	35.90	2.0	1.6	0.4	3.0	2.2

^aUncertainties $\beta \pm 0.2$.

^b $\beta_o = (\alpha_o + 1)/2$.

^c $\alpha_p = -1 + 2\beta$.

5.1 Slope of $N(R)$

Observed slopes for the H II LFs typically fall in the range $1.5 \lesssim a \lesssim 2.5$ (e.g., Kennicutt *et al.* 1989), and thus imply a similar range in β . We therefore see that we are indeed in the regime $\beta > \frac{2}{3}$ for which we developed the solutions of $N(R)$ above. Focusing again on the superbubble size distribution for $R < R_e$ (equation 42), we find that such values of β imply an $N(R)$ that is dominated by the term with a dependence of $R^{1-2\beta}$. This term describes stalled shells, including those that are in the survival phase after stalling. Our assumed range of β therefore implies a range in slope α , where $N(R) \propto R^{-\alpha}$, of $2 \lesssim \alpha \lesssim 4$.

Figures 3 and 4 show the histograms of HI hole radii in pc, with Figure 3 binned and displayed linearly, and Figure 4 binned and displayed logarithmically. The data in the figures are superimposed with a dashed line showing a least-squares, power-law fit to the data, of slope α_o . This fit was derived from the logarithmic binning in Figure 4, weighted by the inverse of the root- N errors shown in the figure. Bins without error bars are deemed incomplete and were not included in the fit. We also show the prediction of equation 42 in the solid line, having a slope of essentially $\alpha_p = 1 - 2\beta$. Where known, the HI scale height h is indicated with the vertical dotted line, and the HI survey resolution limit is indicated by the vertical dashed line. Values for α_p are given in Table 2, and for convenient comparison, α_o is listed there as well. We also give values for $\beta_o = (\alpha_o + 1)/2$, predicted from the observed α_o , and the uncertainties $\sigma(\beta_o)$ derived from the formal standard deviation on the fit to α_o .

The comparison between predicted and observed slopes is surprisingly good, and is in agreement within the errors for all the galaxies. The SMC has by far the most reliable and complete HI data, and shows $\alpha_p = 2.8 \pm 0.4$, in excellent agreement with $\alpha_o = 2.7 \pm 0.6$. This is more vividly demonstrated by the comparison that $\beta = 1.9 \pm 0.2$, taken from the H II LF, which is in superb agreement with $\beta_o = 1.9 \pm 0.3$, predicted by the HI hole size distribution. The agreement for the SMC is extremely encouraging, given the high level of completeness in the data for this galaxy (see below). While the agreements for Holmberg II, M31, and M33 are additionally gratifying, unfortunately the poor statistics in the data for those galaxies render the comparison less significant.

5.2 Normalization of $N(R)$

The normalization of $N(R)$ depends on the coefficient A of the MLF and the superbubble formation rate ψ . A can be calculated by integrating equation 1 over the relevant range of L . This yields,

$$A = (1 - \beta) \left[L_e^{1-\beta} - L_{\text{min}}^{1-\beta} \right]^{-1}. \quad (68)$$

The lower limit of integration, L_{min} , is the power associated with a single SN explosion. In the standard treatment for the SN power used above, this implies $L_{\text{min}} = E_{51}/t_e = 8 \times 10^{35} \text{ erg s}^{-1}$, where $E_{51} = 10^{51} \text{ erg}$, the assumed energy of a single SN explosion. In this limit, the approximation breaks down in its treatment of an energy input over the period t_e , and we will address this point in §5.3 below. However, this does provide a useful value for L_{min} . We use L_e as the upper limit of integration because we are comparing the observations to equation 42, which applies only for $R < R_e$, or equivalently, $L < L_e$. Since $N(R)$ is dominated by stalled objects at small R , and therefore small L , equation 68 is not sensitive to the choice of upper limit.

The superbubble formation rate $\psi = N_{\text{tot}}/(t_e + t_s)$, where N_{tot} is the total number of superbubbles at any given time. This assumes ψ to be constant over the timescale of $t_e = 40 \text{ Myr}$, relevant to the observations. As can be seen in Table 1, it generally appears that for the galaxies examined, $N_{\text{HII}} > N_{\text{HI}}$. This is presumably a selection effect due to the sensitivity and resolution limits of the HI surveys. The incompleteness is also better understood for N_{HII} than N_{HI} , so we will therefore estimate N_{tot} from N_{HII} . Since \mathcal{L} for the nebulae diminishes to below the detection limit well before t_e , we must apply a correction to N_{HII} to obtain the total number of superbubbles N_{tot} , which we estimate as follows.

Unsurprisingly, the proximity of the SMC, surveyed at high sensitivity in HI (Staveley-Smith *et al.* 1996), reveals a much greater surface density of superbubbles than the other galaxies. $N_{\text{HI}} > N_{\text{HII}}$ for the SMC, which, as mentioned above, would

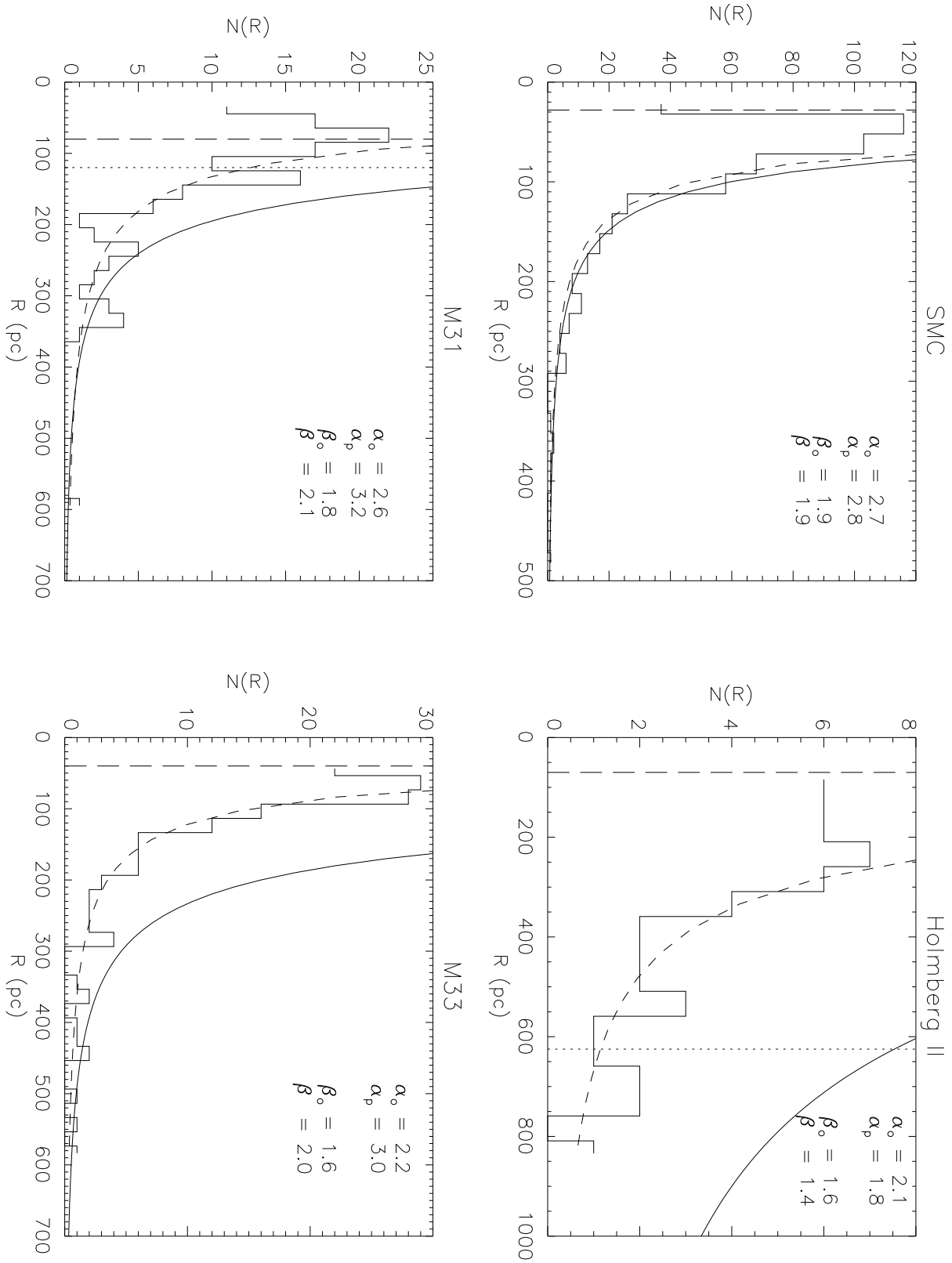


Figure 3. Histogram of HI hole radii. Power-law fits to the data with slope α_o are shown with the dashed line, from which inferred values of the MLF slope β_o are computed. The solid lines show the predicted size distribution with slope α_p , computed with the value of β from the HII LFs. HI scale heights, where known, are indicated by the vertical dotted lines, and the survey resolution limits are shown by the vertical long-dashed lines.

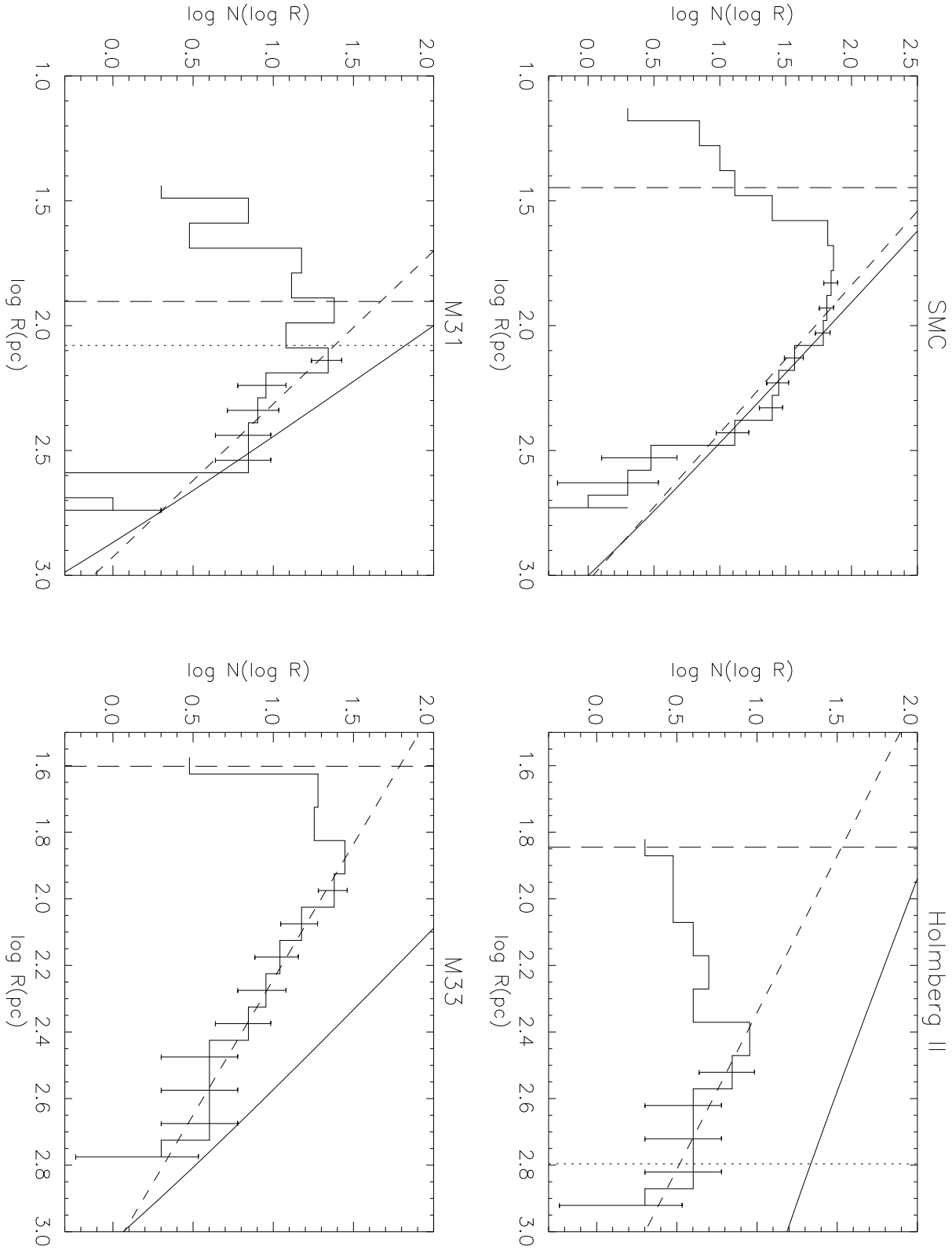


Figure 4. Same as Figure 3, displayed and binned on a logarithmic scale. Data bins without error bars were not included in deriving the fitted relation (short-dashed line). [Note that the slope of $\log N(\log R)$ vs. $\log R$ is $1 - \alpha_0$.]

be expected generally. Furthermore, the excellent agreement in observed and predicted slope for $N(R)$ suggests that for the SMC, we can simply normalize the predicted $N(R)$ to the data, obtain N_{tot} , and thereby estimate $N_{\text{tot}}/N_{\text{HII}}$. Assuming that the shell census for the SMC is complete for $R > 100$ pc, we can use the integral $\int_{100\text{pc}}^{R_e} N(R) dR$ to normalize the prediction for $N(R)$ and obtain N_{tot} . Integrating equation 42 yields,

$$N_{\text{tot}} = \frac{N_{100}}{2A} \frac{R_e^{2-2\beta}}{L_e^{1-\beta}} (2-2\beta) \left[R_e^{2-2\beta} - R_{100}^{2-2\beta} \right]^{-1}, \quad (69)$$

where $N_{100} = 159$ is the number of SMC shells with $R > R_{100}$, which is 100 pc. Using $\beta = 1.9$ from the HII LF for the SMC (Tables 1 and 2), this yields $N_{\text{tot}} = 1.95 \times 10^3$, and $\psi = 43 \text{ Myr}^{-1}$ with $t_e + t_s = 45 \text{ Myr}$. We therefore obtain $N_{\text{tot}}/N_{\text{HII}} = 21.0$.

General application of this conversion factor does assume that N_{HI} is essentially complete at $R > R_{100}$, although Staveley-Smith *et al.* (1996) believe there is still substantial incompleteness in their data. However, based on the following, we expect that most of the incompleteness is in the small shells, where the resolution limit of 28 pc becomes important. The SMC ratio of $N_{\text{tot}}/N_{\text{HII}} = 21.0$ implies a typical HII region age of 2.1 Myr, for $t_e + t_s = 45 \text{ Myr}$. We note that if HII regions fade according to the power law prescription (equation 65), the average age of nebulae that are observed before fading below a given completeness limit L_c is given by,

$$\bar{t} = \frac{\int_{L_c}^{\infty} \phi(L) t_c(L) dL}{\int_{L_c}^{\infty} \phi(L) dL}, \quad (70)$$

where $t_c = t_i \left(\frac{L}{L_c} \right)^{-1/\eta}$, so that

$$\bar{t} = \left(\frac{\beta - 1}{\beta - 1 - \frac{1}{\eta}} \right) t_i. \quad (71)$$

The mean age \bar{t} is therefore close to t_i because, with the assumed luminosity evolution that fades strongly after t_i , most of the nebulae will spend only a short fraction of their lifetimes in the fading period before disappearing below the completeness limit. For $\beta = 2$, and taking $t_{\text{ms}}(m_{\text{up}})$ to be $t_i = 2.8 \text{ Myr}$ (*e.g.*, Maeder 1990), equation 71 gives $\bar{t} = 2.2 \text{ Myr}$. Thus the mean HII region age based on our assumptions for timescales and luminosity evolution is in excellent agreement with that of 2.1 Myr implied by the SMC data. We are therefore fairly confident that this ratio of $N_{\text{tot}}/N_{\text{HII}}$ may be used as a reasonable conversion factor to obtain N_{tot} . However, we caution that applying the SMC conversion universally assumes the same relative extinction for nebulae in all the galaxies, which is actually likely to vary. The SMC itself appears to have a large column depth of HI (Staveley-Smith *et al.* 1996), and may have a disproportionate fraction of HII regions lost below the completeness limit of the nebular census.

Using $N_{\text{tot}}/N_{\text{HII}} = 21.0$, we estimate N_{tot} for the remaining galaxies. These are listed in Table 2, along with the resultant ψ and MLF parameters A , β . These parameters can now be used in equation 42 to quantitatively predict the superbubble size distributions for each galaxy, that are shown in Figures 3 and 4.

The relative normalizations of the observations and predictions are in worse agreement than the slopes, reflecting the huge incompleteness in the HI hole data described above. There is also significant uncertainty in the conversion $N_{\text{tot}}/N_{\text{HII}}$, which as we argued, may be slightly higher in the SMC than the other galaxies. Hence the disparity in the total numbers of predicted and observed $N(R)$ may be slightly exaggerated in these other galaxies.

One check on the critical parameter ψ and resulting normalizations is a calculation of the expected core-collapse (Type II + Ib) SN rate, $\psi_{\text{SN}} = \bar{N}_{\text{SN}}\psi$, that is implied by our analysis. The average number of SNe per cluster \bar{N}_{SN} , can be estimated as

$$\bar{N}_{\text{SN}} = \frac{\bar{L}t_e}{E_{51}} = \frac{\bar{L}}{L_{\text{min}}}. \quad (72)$$

This again assumes that the stellar winds contribute little to L . The mean $\log \bar{L}$ is set by β for constant L_{min} . We tabulate $\log \bar{L}$ and ψ_{SN} for the galaxies in Table 3, with SN rates given in $\text{SNu} = \text{number of SNe per } 10^{10} L_{\odot}(B) \text{ per } 100 \text{ yr}$. Table 3 also shows for comparison the empirically estimated core-collapse SN rates $\psi_{\text{SN}}(\text{obs})$ as reviewed by van den Bergh & Tammann (1991). There is a factor of a few uncertainty in these rates, but reassuringly, our computed $\psi_{\text{SN}}(\beta)$ are in reasonable agreement or less than the empirical estimates. Our normalizations for $N(R)$ are therefore generally quite consistent with the expected SN rates, and at least are not substantial overestimates.

5.3 Peak in $N(R)$

The observations show a peak in $N(R)$, which is undoubtedly related to the resolution limit of the HI surveys. However, it turns out that the theoretical size distribution peaks at similar radii. Since $N(R)$ is dominated by the stalled shells, the minimum stalled $R = R_{\text{min}}$ is simply the stall radius corresponding to the minimum input power L_{min} , which corresponds

Table 3. Supernova Rates

Galaxy	$M_B(\text{Ref.})^a$	$\bar{L}(\beta)$ (erg s^{-1})	$\psi_{\text{SN}}(\beta)$ (SNU)	$\psi_{\text{SN}}(\text{obs})^b$ (SNU)
SMC	-15.7 (1)	8.6×10^{36}	1.1	1.3 – 3.0
Holm II	-16.6 (2)	6.3×10^{37}	2.5	(2.9)
M31	-21.6 (3)	4.8×10^{36}	0.006	0.03
M33	-18.4 (1)	6.3×10^{36}	0.19	0.4

^aReferences for M_B :

- (1) van den Bergh & Tammann (1991)
- (2) Puche *et al.* (1992)
- (3) Sandage & Tammann (1987)

^bFrom van den Bergh & Tammann (1991); value for Holmberg II is that estimated for galaxies of type Sdm – Im, with $H_0 = 75 \text{ km s}^{-1} \text{ Mpc}^{-1}$.

to that of individual SNe, as shown above. For $R < R_{\min}$, $N(R) \propto R^{2/3}$, as given by equation 39 (§3.3). Our value of $L_{\min} = 8 \times 10^{35} \text{ erg s}^{-1}$ thus yields $R_{\min} = 30 \text{ pc}$ (equation 29). However, the evolution of individual SNRs is rather different from that of superbubbles with continuous energy injection. Our limiting extreme in superbubble evolution yields an SNR stall radius that is a factor of 2 or 3 less than estimates by Cioffi & Shull (1991), who consider more realistic SNR evolution and slightly different ISM parameters. Consideration of an ambient magnetic field by Slavin & Cox (1992) produces maximum radii of $\sim 50 \text{ pc}$, 20% less than unmagnetized evolution. So it would seem that the peak in the size distribution of HI holes should fall between 30 and 100 pc.

The HI surveys seem to suggest a peak of $\lesssim 50 \text{ pc}$. The resolution limits have similar values, so at present it is unclear whether $N(R)$ continues to increase toward smaller radii, or whether the peak is actually falling in the expected range. It is interesting that for the SMC in particular, which has the highest quality data and resolution limit of 28 pc, that $N(R)$ still shows no sign of falling off at low values. However, our treatment of superbubble evolution assumes a universal lifetime for all shells of $t_e = 40 \text{ Myr}$. Again, this assumption breaks down for individual SNRs. The peak in the size distribution may be affected by their shorter lifetime and shrinkage by the ambient pressure or magnetic tension (Ferrière *et al.* 1991) after the maximum sizes are attained. At any rate, assuming that the peak radius does actually correspond to the typical endstage radius for individual SNRs, the observed peak value of R could help constrain SNR evolution, ISM conditions and/or the typical SN energy in galaxies for which it is well-determined.

6 SUPERBUBBLES AND THE ISM

It is extremely encouraging that the predictions and observations for the slope of $N(R)$ are in agreement for the HI holes in these galaxies, especially the largely complete sample for the SMC. Since these superbubbles constitute one of the principal forms of structure in the ISM, the implication is that its large-scale structuring is indeed most likely determined largely by these OB superbubbles. Furthermore, a strong agreement, as might be the case for the SMC, implies that *no additional fundamental process is necessary to explain the creation and evolution of observed HI holes*.

The agreement of our relation for $N(R)$ with the SMC data additionally suggests that most of the simplifying assumptions made in §2.1, such as constant IMF, single-burst star formation in clusters, uniform ambient medium, etc. are practical in this analysis. We have confirmed that the MLF spectrum, in particular, is a critical parameter to $N(R)$, and affects the resulting ISM structure. In comparing with Galactic HI observations, Bregman, Kelson, & Ashe (1993) found discrepancies in ISM structure functions modeled from a uniform size distribution of HI holes. It would be interesting to see whether accounting for a power-law $N(R)$, as required by the MLF, can more accurately reproduce the observations.

We do caution that Staveley-Smith *et al.* (1996) note a strong coherence in the dynamical ages of the SMC shells, suggesting a short formation burst. This is in contradiction with our assumption of constant ψ . We predicted the form of $N(R)$ for a single burst in §3.2, finding that $N(R) \propto R^{1-2\beta}$ for $R < R_f(t_b)$, where t_b is the age of the burst. For $R > R_f(t_b)$, $N(R) \propto R^{4-5\beta}$, corresponding to growing shells, with a factor $\frac{5}{2}$ discontinuous jump. Staveley-Smith *et al.* (1996) find $t_b = 5 \text{ Myr}$ for a burst scenario, yielding $R_f = 160 \text{ pc}$. The data in Figure 3 extend to twice this radius, with no suggestion of the predicted discontinuity. The observations therefore appear to be inconsistent with this single burst. Since the constant formation model implies that most shells have stalled, we suggest that the Staveley-Smith *et al.* (1996) result may stem from this majority of stalled objects having spurious expansion velocities attributed to them. The stalled shell walls may instead reflect random ISM velocities. We plan a followup study of the distribution in expansion velocities, which will clarify this issue.

As is apparent in Figure 4, the two disk galaxies, M31 and M33, show greater disagreement in predicted and observed slopes of $N(R)$ than do Holmberg II and the SMC, which are both Magellanic irregulars. Owing to the apparent enormous

incompleteness in the HI hole samples and high uncertainties on the fit to $N(R)$, we cannot attribute significance to this possible correlation between galaxy morphology and relative agreement in slopes. Nevertheless, the contrast in relative agreement between the different galaxy types is suggestive and interesting. Since the gas distribution and dynamical processes in spiral galaxies differ from those of dwarf irregulars, it is reasonable to suspect that superbubble evolution is likely to differ between these morphological types of galaxies. For example, Ferrière (1995) shows that the three-dimensional evolution of superbubbles in an exponential gas disk is quite different from the spatially uniform expansion we have assumed here. Differential rotation in the disks and radial effects such as the distribution of gas and star-forming regions are other examples of factors that are likely to be important in spiral galaxies.

6.1 The Smallest and Largest Shells

The regimes where we expect significant disagreement between the prediction and observations would be at the extremes in radius. As described above, the smallest shells should correspond mostly to individual SNRs, whose evolution is significantly different from what is assumed by equation 24. The continuous wind approximation is also likely to break down for superbubbles created by only a few discrete SNe. The sizes of such objects may be underestimated since observational and theoretical evidence suggests that many SNRs strike the superbubble walls, therefore converting their energy into direct kinetic impulses and shell X-ray radiation instead of thermal energy in the shell interior (*e.g.*, Oey 1996; Chu & Mac Low 1990; Franco *et al.* 1991). In addition, we may expect a significant contribution from Type Ia SNe. However, the addition of Type Ia SNRs to $N(R)$ would cause a jump in the peak predicted at R_{\min} . There is as yet no evidence for such a jump, again demonstrating that R_{\min} itself is empirically not yet apparent.

At large R , we expect the HI scale height h to be a critical factor in the evolution of the superbubbles. The growth of the superbubble radius to h allows the interior hot gas to break out of the galactic disk and depressurize the shells. Heiles (1990) assumed a bimodal evolution, where for $R < h$, the shell growth followed $R \propto t^{3/5}$ given by equation 24; and for $R > h$, the growth was described by a coasting, momentum-conserving phase with $R \propto t^{1/3}$ (cylindrical geometry). Such an effect should cause a steepening in slope α of the size distribution at large R : since these shells can no longer grow as large as they would have done adiabatically, they accumulate at smaller final radii. However, the observations are showing slopes that are generally shallower than α_p , rather than steeper, thus the limiting effect of h is not apparent in the data for these galaxies. As seen in Figure 3, $N(R)$ does appear rather irregular in M31, especially at R a few tens of pc above h , hinting at the possible effect of breakouts. However, for M33 and the SMC, $N(R)$ follows a power-law distribution quite smoothly, even for $R > h$. There is a hint of a break in the SMC data around 300 pc, that could possibly correspond to an equivalent h , which is indeterminate for this galaxy.

It seems likely that some other mechanism might also create superbubbles with $R > h$, generating an excess of large superbubbles, and thereby flattening the observed slope α_o of the size distribution. As discussed by Heiles (1990), among others, the two principal candidate mechanisms are propagating star formation and infalling high-velocity clouds (HVCs). Propagating star formation (*e.g.*, McCray & Kafatos 1987) produces generations of OB associations in close spatial proximity, thereby increasing the mechanical power L and extending the duration of energy input beyond t_e . This can therefore lead to supergiant shells with radii larger than are likely to be due to individual OB associations. Impacts by HVCs have also been demonstrated to produce shell structures with radii of $10^2 - 10^3$ pc (*e.g.*, Tenorio-Tagle *et al.* 1987; Rand & Stone 1996). But these mechanisms, if applicable, apparently do not create enough shells to clearly distinguish their contribution to the superbubble size distribution in the current data, and blend smoothly with $N(R)$ predicted by the MLF for OB associations.

It is also quite possible that many of the larger shells are created by the merging of smaller ones. This would cause a flattening in the slope α of the size distribution, since smaller shells would be eliminated to combine larger ones. The inter-cluster distance for OB associations is typically a few hundred pc in these galaxies, so we expect merging to be important for shells with radii larger than this range. We note that the observed slopes are all flatter than predicted, with the exception of that for Holmberg II, which has by far the worst uncertainty. We commented above on the possibility of disagreement between predicted and observed slope in the spiral galaxies versus the Magellanic irregulars; another potential explanation for such a discrepancy is that the concentration of star forming regions in the spiral arms enhances merging and propagating star formation, preferentially encouraging the production of the very large shells and thereby flattening the resultant α .

6.2 Porosity of the ISM

The favorable comparison between the observations and prediction encourage us to apply this analysis to the global structure of the ISM in galaxies. A fundamental outstanding issue is the relative importance of hot, coronal gas, which presumably originates in superbubbles and Type Ia SNRs, in relation to the cooler phases of the ISM. This question is traditionally addressed by means of the porosity parameter Q (Cox & Smith 1974), which is the ratio of total volume or area occupied by superbubbles to the total volume or area of the host galaxy. Following directly on the preceding section, we can also evaluate the degree of shell merging or overlap by examining Q .

Table 4. Porosity Parameters

Galaxy	R_g (kpc)	Predicted		Observed	
		Q_{2D}	Q_{3D}	Q_{2D}	Q_{3D}
SMC	2	2.1	0.3	1.6	0.1
Holm II	7	1.5	1.2	0.1	0.08
M31	17	0.03	0.06	0.01	0.02
M33	7	0.3	0.9	0.08	0.2

Following Heiles (1987, 1990), we compute both the two-dimensional Q_{2D} , and volume porosity Q_{3D} . Q_{2D} is especially appropriate for the disk distribution of OB associations in spiral galaxies. We have,

$$Q_{2D} = A_g^{-1} \int A_b N(A_b) dA_b \quad , \quad (73)$$

where $A_b = \pi R^2$ is the projected superbubble area, and A_g is the area of the galactic disk. Rewriting this expression in terms of $N(R) dR$:

$$Q_{2D} = (\pi R_g)^{-2} \int_{R_{\min}}^{R_e} \pi R^2 N(R) dR \quad , \quad (74)$$

recalling that we are in the regime $R < R_e$, $\beta > \frac{2}{3}$ for the standard model. We obtain,

$$Q_{2D} = R_g^{-2} A \psi L_e^{1-\beta} R_e^2 \left\{ \left[\frac{B}{4-2\beta} + \frac{C}{5-2\beta} \right] - \left(\frac{R_{\min}}{R_e} \right)^{4-2\beta} \left[\frac{B}{4-2\beta} + \frac{C}{5-2\beta} \left(\frac{R_{\min}}{R_e} \right) \right] \right\} \quad , \quad (75)$$

where R_g is the radius of the galactic disk, and

$$B = 2(t_e + t_s) \quad (76)$$

$$C = \frac{9-6\beta}{-2+3\beta} t_e \quad . \quad (77)$$

For $\beta > 2$, Q_{2D} is dominated by R_{\min} , but for $\beta < 2$, the largest shells dominate. Interestingly, the relevant values of β fall in this transition. Thus for some galaxies, the few largest shells dominate Q_{2D} , whereas in others it is dominated by the many individual SNRs. For those with $\beta \sim 2$, the relative superbubble sizes contribute fairly equally in determining Q_{2D} .

The C term, corresponding to the term in equation 42 with dependence $R^{2-2\beta}$, is small for parameters of interest, and will only dominate for $\beta < 1$. We may therefore approximate,

$$Q_{2D} \simeq R_g^{-2} A \psi L_e^{1-\beta} R_e^2 \frac{2(t_e + t_s)}{4-2\beta} \left[1 - \left(\frac{R_{\min}}{R_e} \right)^{4-2\beta} \right] \quad . \quad (78)$$

By analogy, we also compute the three-dimensional porosity parameter:

$$Q_{3D} = \frac{2}{3hR_g^2} A \psi L_e^{1-\beta} R_e^3 \left\{ \left[\frac{B}{5-2\beta} + \frac{C}{6-2\beta} \right] - \left(\frac{R_{\min}}{R_e} \right)^{5-2\beta} \left[\frac{B}{5-2\beta} + \frac{C}{6-2\beta} \left(\frac{R_{\min}}{R_e} \right) \right] \right\} \quad , \quad (79)$$

using the HI scale height h as the relevant galactic vertical extent. R_{\min} dominates for $\beta > 2.5$, so Q_{3D} is almost always dominated by the largest shells. Again, we find that the C term is usually small, dominating only for $\beta \lesssim 1$, so we may approximate,

$$Q_{3D} \simeq \frac{2}{3hR_g^2} A \psi L_e^{1-\beta} R_e^3 \frac{2(t_e + t_s)}{5-2\beta} \left[1 - \left(\frac{R_{\min}}{R_e} \right)^{5-2\beta} \right] \quad . \quad (80)$$

We take R_g to be the distance out to which HI holes are detected in these galaxies. The adopted R_g , and resultant Q_{2D} and Q_{3D} are given in Table 4. These are the exact values, computed from equations 75 and 79. We also list the observed values of Q_{2D} and Q_{3D} , computed from the HI holes with $R > R_{\min}$. We caution that the predicted porosities could be overestimates, since equations 75 and 79 assume a size distribution extending to $R_e = 1300$ pc. Because of the small numbers of large shells predicted, it is unclear whether the distributions indeed may be considered to extend to R_e .

For M31 and M33, we take Q_{2D} to be the relevant porosity parameter, and for the SMC, Q_{3D} . The values in Table 4 of the relevant porosity parameters for these galaxies are all significantly less than 1. We therefore do not expect a great deal of superbubble overlap and merging in these galaxies, thereby limiting the extent and networking of the hot gas that originates within the shells. On the other hand, the predicted porosity parameters for Holmberg II are $\gtrsim 1$. This galaxy has a very large scale height, so both Q_{2D} and Q_{3D} are relevant, as is indicated by their similar values. These predict that Holmberg II, unlike the other galaxies, does have an ISM that is dominated by coronal gas. This supports the expectation

Table 5. Parameters for the Galaxy^a

Model	N_{tot}	ψ (Myr ⁻¹)	$\log A$	β	α_p	$\bar{L}(\beta)$ (erg s ⁻¹)	ψ_{SN}^b (SNu)	$Q_{2\text{D}}$	$Q_{3\text{D}}$
MW96	6.5×10^3	1.4×10^2	35.90	2.0	3.0	6.3×10^{36}	0.05	0.1	0.3
SK89	3.8×10^4	8.5×10^2	46.78	2.3	3.6	3.1×10^{36}	0.14	0.2	0.4
E2.0	4.0×10^5	8.9×10^3	35.90	2.0	3.0	6.3×10^{36}	(3.0)	6.7	19
E2.3	8.0×10^5	1.8×10^4	46.78	2.3	3.6	3.1×10^{36}	(3.0)	3.9	8.1

^aAssuming $R_g = 13$ kpc, $h = 100$ pc, and $L_{\odot,B} = 2.3 \times 10^{10}$.

^bValue for models E2.0 and E2.3 is the empirical estimate of ψ_{SN} for the Galaxy (van den Bergh & Tammann 1991).

that the importance of the HIM depends on the level of star formation relative to galaxy size and interstellar conditions. It is important to keep in mind that, as seen in §5.2, the normalizations of $N(R)$ are uncertain, and these affect the derived porosity parameters, as does the assumption of a distribution extending to R_e . However, given the general consistency with the SN rates, and possible overestimate of the $N_{\text{tot}}/N_{\text{HII}}$ conversion factor, we imagine that the porosities in Table 4 should not be hugely underestimated. Our derived $Q_{2\text{D}}$ nevertheless essentially agree with the values estimated by Heiles (1990) for M31 and M33. His analysis is based on somewhat different criteria with greater uncertainties. For example, he examined primarily superbubbles that break out of the galactic disk, and included an *ad hoc* adjustment in his $\mathcal{L} - N_*$ relation.

Note that the existence of the MLF spectrum, which accounts for the clustering of core-collapse SNe, has a potentially important effect on the porosity. Whereas N_* uniformly distributed SNe will, at their final radii, contribute to $Q_{3\text{D}}$ simply as $N_* L_{\text{min}}^{3/2} \propto N_*$, the same SNe concentrated into one cluster will contribute as $(N_* L_{\text{min}})^{3/2} \propto N_*^{3/2}$ (for $N_* L_{\text{min}} < L_e$; equation 29). Clustered SNe in superbubbles therefore produce a larger $Q_{3\text{D}}$ than the same number of individual SNe. However, this is not the case for $Q_{2\text{D}}$, where for both individual and clustered SNe, $Q_{2\text{D}} \propto N_* L_{\text{min}}$. Although, as we have seen above, the largest shells constitute a larger component of $Q_{2\text{D}}$, the relative degree of clustering will not affect the actual value of $Q_{2\text{D}}$. Ferrière (1995) also finds a strong effect of clustering on $Q_{3\text{D}}$, using a more complex model for shell evolution in an exponential gas disk.

It is also important to bear in mind the contribution of Type Ia SNRs (*e.g.*, Slavin & Cox 1993), although in most star-forming galaxies, these are outnumbered by factors of 3–10 by core-collapse SNe (van den Bergh & Tammann 1991). Heiles (1987) emphasizes that the distribution of Type Ia SNe should vary with galactocentric radius in disk galaxies, owing to the distribution of progenitors, and could therefore cause important radial effects in the ISM porosity. This effect could be a factor in the discrepancy between observed and predicted slopes for M31 and M33. As mentioned in §6.1, the HI data do not yet provide empirical evidence for the contribution of Type Ia SNRs in the galaxies we have examined.

It is interesting to apply our analysis to the porosity of the Milky Way. The HII LF for the Galaxy has been compiled by McKee & Williams (1996; hereafter MW96) and Smith & Kennicutt (1989; hereafter SK89), where both sets of authors used primarily the compiled data of Smith, Biermann, & Mezger (1978). The HII LF estimated by MW96 (their Figure 2), shows a slightly flatter slope of $a = 2.0$, compared to $a = 2.3$ reported by SK89. The data from these papers yield parameters for the Galaxy shown in Table 5. The values of β from the HII LF predict a fairly steep slope for $N(R)$ in the Galaxy of 3.0 and 3.6. For the SK89 data, we base our calculations on an estimated total of 145 HII regions having $\log \mathcal{L} > 37.84$ erg s⁻¹ (see their Figure 1). It is apparent that the predicted SN rates ψ_{SN} are an order of magnitude smaller than the observed ψ_{SN} of ~ 3 SNu estimated for the core-collapse SNe in the Galaxy (van den Bergh & Tammann 1991). We therefore also compute implied parameters based on the empirical SN rate, for $\beta = 2.0$ (model E2.0) and $\beta = 2.3$ (model E2.3). Resulting porosities are computed assuming $R_g \sim 13$ kpc, based on the data of Smith *et al.* (1978), and $h = 100$ pc (Kulkarni & Heiles 1987).

Unfortunately, this discrepancy in the predicted and observed SN rates has a critical impact on the Galactic porosity parameters. As seen in Table 5, the porosity estimates based on the observed Galactic HII LF are consistent with the low porosities estimated for the other galaxies (Table 4). However, the Galactic estimates based on the much larger, observed ψ_{SN} produce porosities $\gg 1$, implying a strong dominance of the hot interstellar component. It is unclear how this discrepancy should be reconciled. On the one hand, the observed Galactic SN rate is consistent with the presumed Hubble type around Sb (van den Bergh & Tammann 1991). On the other hand, van den Bergh finds a similar discrepancy when predicting ψ_{SN} from the local IMF, which also underestimates the observed ψ_{SN} by an order of magnitude (van den Bergh & Tammann 1991). We note that Tammann does not find such a discrepancy, and also that MW96 do find consistency between their HII LF and the Galactic SN rate. It is interesting to note that the only other Sb galaxy in our study, M31, shows a similar, but smaller, discrepancy in observed and predicted ψ_{SN} .

Other authors have estimated the porosity of the Galaxy based on similar analyses. Ferrière (1995) finds $Q_{3\text{D}} \sim 0.2$ based on a more complex, 3D model for shell evolution in an exponential gas disk, including an important shell contraction phase. Slavin & Cox (1993) estimate a value of $Q_{3\text{D}} = 0.18$ for individual SNRs, but exclude the contribution of larger superbubbles,

which we found above to dominate the porosity in our analysis. Heiles (1990) estimates $Q_{2D} = 0.30$, ignoring the contribution of shells that do not break out of the Galactic disk. Since the measurements of β for the Galaxy fall in the regime where small shells dominate Q_{2D} , this value is also likely to be a substantial underestimate. Our results seem very broadly consistent with previous studies, but highlight the uncertainties in Galactic parameters. Apparently we have simply restated the problem of whether or not the hot component of the ISM should strongly dominate in the Milky Way, since this argument is based on the observed supernova rate in the Galaxy (Cox & Smith 1974; McKee & Ostriker 1977).

7 CONCLUSION

We have used the standard, adiabatic shell evolution to predict the differential size distribution $N(R)$ for populations of OB superbubbles in a uniform ISM. The results are strongly dependent on the inclusion of a power-law MLF for the OB associations. Another fundamental ingredient is the criterion that the shell growth stalls upon pressure equilibrium with the environment. This condition, along with the given characteristic time t_e , determines the characteristic radius R_e , that divides the superbubble population into two regimes of solutions corresponding to $N(R < R_e)$ and $N(R > R_e)$. R_e and the corresponding L_e therefore make convenient defining criteria for a different scale phenomenon, for example, a starburst event. For the condition of constant shell creation and power-law MLF, in the regime $R < R_e$, $N(R)$ is given by equation 42, which has contributions from growing, stalled, and surviving objects. For reasonable values of the MLF slope $\beta \sim 2 \pm 0.5$, the size distribution is dominated by stalled objects, yielding $N(R) \propto R^{1-2\beta}$. This $R^{1-2\beta}$ dependence appears to be fairly robust, since it applies to the standard, momentum-conserving evolution (Steigman *et al.* 1975) as well. It also describes $N(R)$ for the single-burst creation of shells, for R smaller than the stall radius associated with the burst age. On the other hand, in the regime $R > R_e$, we find the dependence $N(R) \propto R^{4-5\beta}$ (equation 45), a much steeper relation essentially composed of growing objects.

To estimate β , we adopt the observed slope a of the H II LF. However, the observed a could in principle be steeper than the initial β depending on the relation between the luminosity fading of the H II regions and the initial slope β . We investigated this problem for power-law nebular fading, and found the existence of a minimum slope $a_{\min} = 1 + \frac{1}{\eta}$ (equation 67), which is determined by the power-law index η of the fading function. Thus, for $\beta > a_{\min}$, we may indeed adopt $\beta = a$, but for $\beta < a_{\min}$, a provides only an upper limit to β , as the observed slope is indeed steepened to the value a_{\min} . Observed slopes of galactic H II LFs are all greater than the predicted a_{\min} , so these should provide a fairly reliable measure for the slope of the MLF. It will be interesting to see whether a lower cutoff in the distribution of observed a in galaxies will become manifest at a_{\min} . We also found that the existence of this minimum a_{\min} depends on a long-term, power-law nebular fading law, whereas if the H II region luminosities are instantaneously extinguished at a specified age, no a_{\min} will be observed. We also derive a useful expression for the mean H II region age of a complete population of nebulae brighter than a given luminosity. This is given by equation 71, in terms of β and η .

We compared the predicted size distributions with observed HI hole distributions in four galaxies. The recent data for the SMC (Staveley-Smith *et al.* 1996) appear to be largely complete, and show excellent agreement with our predicted relation of $N(R) \propto R^{1-2\beta}$. Despite the fact that our critical assumptions about *e.g.*, the endstage evolution, are highly uncertain and crudely treated, the slope of the size distribution in this galaxy can be entirely explained by our prediction. *No other fundamental processes are necessary to explain the observed HI hole distribution in the SMC.* This furthermore suggests that our assumptions of constant IMF and coeval star formation in OB associations are broadly useful on global scales.

The observed and predicted slopes of $N(R)$ are also in agreement for the three other galaxies we examined. It is premature to draw conclusions based on these other comparisons, since the HI hole data are largely incomplete, as evidenced by the relative numbers of H II regions vs. HI holes. The predicted SN rates based on our analysis also support this conclusion, and are in reasonable agreement with observed rates. However, it is intriguing that the spiral galaxies appear to suggest greater disagreement in the slope of $N(R)$ compared to the Magellanic irregulars. We anticipate that radial and disk properties associated with spiral galaxies should cause differences in the observed superbubble size distributions. The effect of the disk scale height should be especially apparent in these galaxies, limiting the growth of shells at these sizes, yet such an effect is not apparent in the data, which show plenty of shells at larger radii. Processes such as propagating star formation and merging could contribute large objects that counteract the expected dearth of large shells. At present, however, the data for the spiral galaxies, especially M33, are adequately fit by a simple power-law distribution, and there is no strong evidence for a change in characteristics of large superbubbles.

We also predict a peak in the size distribution corresponding to the smallest stalled shells, which would be individual SNRs. The spatial resolution of the data do not yet allow meaningful comparison with prediction. The contribution of Type Ia SNRs, which could be substantial (Heiles 1987), should also be apparent near this peak.

Our derivation is easily applied to estimating the porosity of the ISM. We find that, not including Type Ia SNRs, Q_{2D} is dominated by individual SNRs for $\beta > 2$, but the few largest shells for $\beta < 2$. On the other hand, Q_{3D} is usually dominated by the largest superbubbles, rather than the multitude of small shells and SNRs. Our estimates for the porosities in these

galaxies generally show values substantially < 1 , with the exception of Holmberg II. This therefore predicts that this galaxy would be dominated by a hot interstellar medium, whereas the others would not. Furthermore, merging would not be expected to be a dominant process in the galaxies with porosities $\ll 1$, although merging could still flatten the slope of $N(R)$ if it is encouraged by spatially clustered shell distributions. Our porosity estimates for these external galaxies are in good agreement with previous calculations (*e.g.*, Heiles 1990), with the caveat that they are dependent on the normalizations for $N(R)$.

However, in predicting the SN rate and porosity of the Milky Way, we find a critical discrepancy between the predicted and observed SN rates: ψ_{SN} based on the observed H II LF underestimates the observed value by an order of magnitude. The predicted value of ψ_{SN} leads to porosities < 1 , similar to results for the other galaxies. However, the observed SN rate yields porosities $\gg 1$, implying a strong dominance of the HIM. It is unclear how this discrepancy should be reconciled, since we have simply recast this pre-existing problem for the Galaxy.

Our results suggest that OB superbubbles are indeed a dominant source of structure in the ISM of galaxies. We used the simplest and crudest formulations to derive the superbubble size distribution, with the aim of identifying dominant processes and evolutionary features. The agreement of this derived prediction with the high-quality SMC data is unexpectedly excellent and encouraging. This tentatively suggests that we have fairly successfully identified the basic features of shell evolution, ISM parameters, and stellar parameters that are relevant to the global structure and evolution of superbubbles. As new, high-resolution HI data become available for more galaxies (*e.g.*, Thilker 1997; Kim *et al.* 1997), we will be able to more rigorously test these results and distinguish unresolved issues.

ACKNOWLEDGMENTS

We have enjoyed discussions with many people, both in Cambridge and in the course of two meetings. It is a pleasure to thank Eric Blackman, Don Cox, Laurent Drissen, Pepe Franco, Despina Hatzidimitriou, Claus Leitherer, Carmelle Robert, John Scalo, Mike Shull, and Guillermo Tenorio-Tagle. We are also grateful to Lister Staveley-Smith for providing access to the SMC HI data in advance of publication.

REFERENCES

- Banfi M., Rampazzo R., Chincarini G., Henry R. B. C. 1993, AA, 280, 373
 Beltrametti M., Tenorio-Tagle G., Yorke H. W. 1982, AA, 112, 1
 Bregman J. N., Kelson D. D., Ashe G. A. 1993, ApJ, 409, 682
 Brinks E., Bajaja E. 1986, AA, 169, 14
 Chu Y.-H. & Mac Low M.-M. 1990, ApJ, 365, 510
 Cioffi D. F., Shull J. M. 1991, ApJ, 367, 96
 Clarke C. J. 1996, MNRAS, 283, 353
 Cox D. P. & Smith B. W. 1974, ApJL, 189, L105
 Deul E. R., den Hartog R. H. 1990, AA, 229, 362
 Drissen L., Moffat A. F. J., Walborn N. R., & Shara M. R. 1995, AJ, 110, 2235
 Dyson J. E. 1977, AA, 59, 161
 Ferrière K. 1995, ApJ, 441, 281
 Ferrière K. M., Mac Low M.-M., Zweibel E. G. 1991, ApJ, 375, 239
 Field G. B., Goldsmith D. W., & Habing H. J. 1969, ApJL, 155, L149
 Franco J., Tenorio-Tagle G., Bodenheimer P., & Różyczka, M. 1991, PASP, 103, 803
 García-Segura G. & Mac Low M.-M. 1995, ApJ, 455, 145
 García-Segura G. & Franco J. 1996, ApJ, 469, 171
 Heiles C. 1984, ApJS, 55, 585
 Heiles C. 1987, ApJ, 315, 555
 Heiles C. 1990, ApJ, 354, 483
 Hodge P., Strobel N. V., & Kennicutt R. C. 1994, PASP, 106, 309
 Hughes J. P., Helfand D. J., Kahn S. M. 1984, ApJ, 281, L25
 Kennicutt R. C., Bresolin F., Bomans D. J., Bothun G. D., & Thompson I. B. 1995, AJ, 109, 594
 Kennicutt R. C., Edgar B. K., Hodge P. W. 1989, ApJ, 337, 761
 Kim S., Staveley-Smith L., Sault R. J., Kesteven M. J., McConnell D., Freeman K. C. 1997, PASA, in press
 Kulkarni S. & Heiles C. 1987, in *Interstellar Processes*, D. J. Hollenbach & H. A. Thronson (eds.), Dordrecht: Reidel, 87
 Leitherer C. 1990, ApJS, 73, 1
 Leitherer C., Heckman T. M. 1995, ApJS, 96, 9
 Mac Low M.-M. & McCray R. 1988, ApJ, 324, 776
 Maeder A. 1990, AAS, 84, 139
 Maeder A., Meynet G. 1988, AAS, 76, 411
 Magnier E. A., Chu Y.-H., Points S. D., Hwang U., & Smith R. C. 1996, ApJ, 464, 829
 Massey P., Johnson K. E., & DeGioia-Eastwood K., 1995, ApJ, 454, 151
 Massey P., Lang C. C., DeGioia-Eastwood K., & Garmany C. D. 1995, ApJ, 438, 188

- McCray R. & Kafatos M. 1987, ApJ, 317, 190
McKee C. F. & Ostriker J. P. 1977, ApJ, 218, 148
McKee C. F. & Williams J. P. 1997, ApJ, 476, 144
Oey M. S. 1996, ApJ, 467, 666
Oey M. S. & Massey P. 1995, ApJ, 452, 210
Panagia N. 1973, AJ, 78, 929
Pikel'ner S. B. 1968, Astrophys. Lett. 2, 97
Puche D., Westpfahl D., Brinks E., Roy J.-R. 1992, AJ, 103, 1841
Rand R. J., Stone J. M. 1996, AJ, 111, 190
Salpeter E. E. 1955, ApJ, 121, 161
Sandage A., Tammann G. A. 1987, *A Revised Shapley-Ames Catalog of Bright Galaxies*, Carnegie Institution of Washington, (Washington, DC)
Schaerer D., Meynet G., Maeder A., & Schaller G. 1993, AAS, 98, 523
Shull J. M., Saken J. M. 1995, ApJ, 444, 663
Slavin J. D. & Cox D. P. 1992, ApJ, 392, 131
Slavin J. D. & Cox D. P. 1993, ApJ, 417, 187
Smith L. F., Biermann P., & Mezger P. G. 1978, AA, 66, 65
Smith T. R. & Kennicutt R. C. 1989, PASP, 101, 649
Staveley-Smith L., Sault R. J., Hatzidimitriou D., Kesteven M. J., McConnell D. 1997, MNRAS, in press
Steigman G., Strittmatter P. A., Williams R. E. 1975, ApJ, 198, 575
Tenorio-Tagle G., Franco J., Bodenheimer P., Różyczka, M. 1987, AA, 179, 219
Thilker D. 1997, Ph.D. Thesis, New Mexico State University, in preparation
Vacca W. D., Garmany C. D., Shull J. M. 1996, ApJ, 460, 914
van den Bergh S., Tammann G. A. 1991, ARAA, 29, 363
von Hippel T., Bothun G. 1990, AJ, 100, 403
Weaver R., McCray R., Castor J., Shapiro P., Moore R. 1977, ApJ, 218, 377